FGCaMP7 Genetically Encoded Calcium Indicator

Subjects: Biochemistry & Molecular Biology

Contributor: Fedor Subach

Genetically encoded calcium indicators (GECIs) have become a widespread tool for the visualization of neuronal activity. As compared to popular GCaMP GECIs, the FGCaMP indicator benefits from calmodulin from the *Aspergillus niger* fungus, which prevent its interaction with the intracellular environment. However, FGCaMP exhibits a two-phase fluorescence behavior with the variation of calcium ion concentration, has moderate sensitivity in neurons (as compared to the GCaMP6s indicator), and has not been fully characterized in vitro and in vivo. To address these limitations, we developed an enhanced version of FGCaMP, called FGCaMP7. FGCaMP7 preserves the ratiometric phenotype of FGCaMP, with a 3.1-fold larger ratiometric dynamic range in vitro. FGCaMP7 demonstrates 2.7- and 8.7-fold greater photostability compared to mEGFP and mTagBFP2 fluorescent proteins in vitro, respectively. The ratiometric response of FGCaMP7 is 1.6- and 1.4-fold higher, compared to the intensiometric response of GCaMP6s, in non-stimulated and stimulated neuronal cultures, respectively. We reveal the inertness of FGCaMP7 to the intracellular environment of HeLa cells using its truncated version with a deleted M13-like peptide; in contrast to the similarly truncated variant of GCaMP6s. We characterize the crystal structure of the parental FGCaMP indicator. Finally, we test the in vivo performance of FGCaMP7 in mouse brain using a two-photon microscope and an NVista miniscope; and in zebrafish using two-color ratiometric confocal imaging.

Keywords: calcium imaging ; genetically encoded calcium indicator ; protein engineering ; crystal structure ; FGCaMP7 ; FGCaMP

1. Structural Characterization of FGCaMP Calcium Indicator

To understand the structural basis underlying FGCaMP functioning and to search for potential mutation hotspots, we determined the crystal structure of the original FGCaMP calcium indicator [1] in its Ca^{2+}-bound state at 3.2 Å resolution (Table S1).

Table S1. Data collection, processing and refinement.

Data collection	
Diffraction source	BL41XU beamline, Spring8
Wavelength (Å)	1.0
Temperature (K)	100
Detector	Pilatus
Crystal-to-detector distance (mm)	570.00
Rotation range per image (°)	0.5
Total rotation range (°)	105
Space group	$P4_32_12$

a, *b*, *c* (Å)	163.56; 163.56; 143.06
α, β, γ (°)	90.0
Average mosaicity (°)	0.45
Unique reflections	33,268 (4353)
Resolution range (Å)	89.94–3.18 (3.34–3.18)
Completeness (%)	100.0 (100.0)
Average redundancy	7.0 (7.0)
⟨*I*/σ(*I*)⟩	13.6 (2.4)
Rmeas (%)	10.6 (94.7)
$CC_{1/2}$	98.5 (72.6)
Refinement	
R_{fact} *(%)*	27.9
$R_{free.}$ *(%)*	34.8
Bonds (Å)	0.01
Angles (°)	1.69
Ramachandran plot	
Most favored (%)	94.5
Allowed (%)	3.6
No. atoms	
Protein	6427
Water	3
Chromophore	44
Calcium ion	10
B-factors (Å²)	

Protein	**89.14**
Water	**45.19**
Chromophore	**77.44**
Calcium ion	**103.59**

Values in parenthesis are for the highest-resolution shell.

Like all GCaMP-like calcium indicators, according to its crystal structure, FGCaMP represents two domains: a cpEGFP moiety and a CaM/M13-peptide complex with four bound calcium ions (Figure S1, Figure 1a).

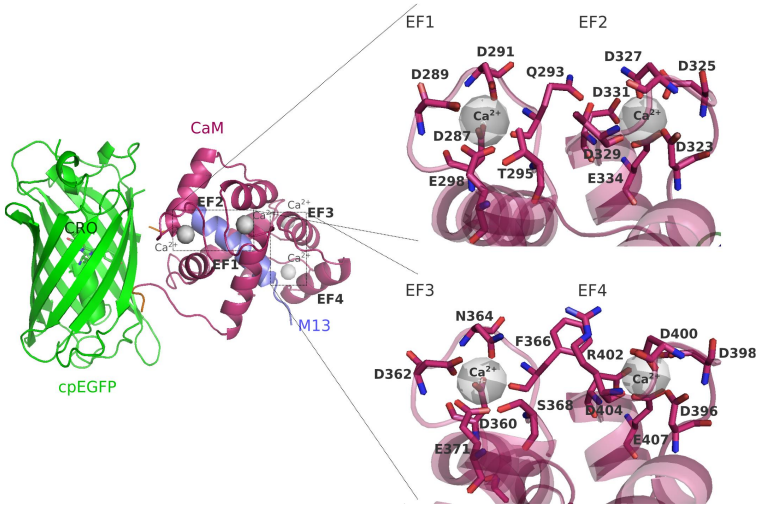

Figure S1. Crystal structure of FGCaMP indicator in Ca^{2+}-bound state (PDB 6XU4). **(Left)** β-barrel of cpEGFP is shown as a green cylinder, Ca^{2+} ions are shown as grey spheres, M13-peptide and CaM are shown in purple and light blue, respectively. Cro: cromophore. **(Right)** Ca^{2+}-binding motives 1 and 2, 3 and 4 (EF1–EF4). Ca^{2+} ions are shown as grey spheres. Ca^{2+}-binding amino acids are indicated.

The cpEGFP moiety contains 11 β-strands forming a β-barrel with chromophore formed by $TYG^{184-186}$ buried inside the barrel. CaM includes 8 α-helixes organized into four calcium-binding motifs (EF1–EF4). Each motif co-ordinates a single calcium ion by six contacts, as typical for calcium-binding domains (Figure S1) [2].

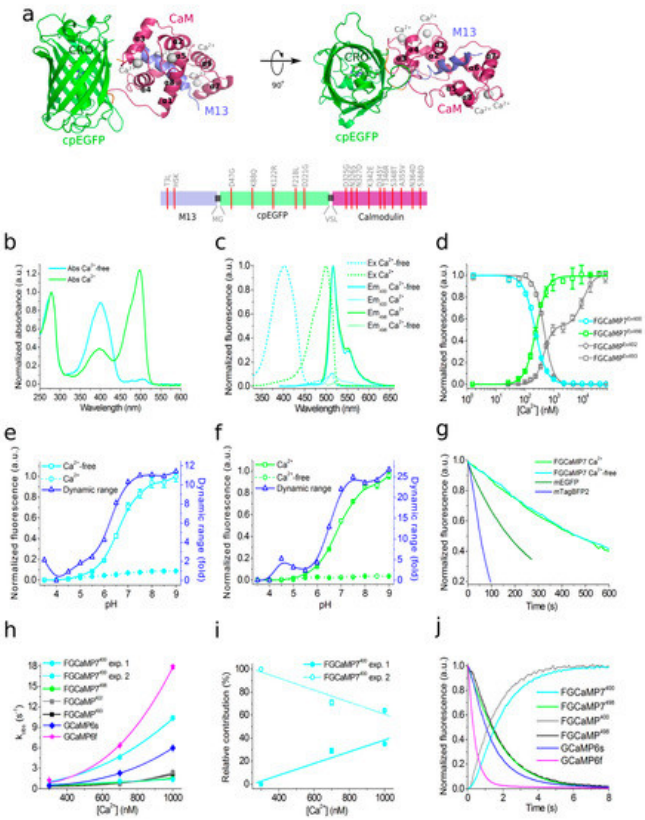

Figure 1. Structure and properties of the FGCaMP7 calcium indicator. (**a**, top) Orthogonal views of the structure of the FGCaMP indicator in Ca^{2+}-bound state (PDB 6XU4). β-barrel of cpEGFP is shown as a green cylinder, Ca^{2+} ions are shown as grey spheres, M13-peptide and CaM are shown in purple and light blue, respectively. α-helices of CaM are indicated. (**a**, bottom) Schematic representation of the FGCaMP7 sequence with mutations relative to the original FGCaMP. The numbering follows that for FGCaMP. (**b**) Absorbance spectra in the presence (39 μM) and the absence of Ca^{2+} ions for FGCaMP7. (**c**) Excitation and emission spectra in the presence (39 μM) and the absence of Ca^{2+} ions for FGCaMP7. (**d**) Ca^{2+} titration curves for FGCaMP and FGCaMP7. (**e**) Fluorescence of FGCaMP7 as a function of pH at 365 nm excitation. (**f**) Fluorescence of FGCaMP7 as a function of pH at 490 nm excitation. (**g**) Photobleaching curves for FGCaMP7 in the presence (39 μM) and the absence of Ca^{2+} ions and for mEGFP and mTagBFP2 fluorescent proteins. The power of light before the objective lens was 7.3 mW/cm^2. (**h**) Observed Ca^{2+}-association rate constants determined from association curves for FGCaMP, FGCaMP7, and control GCaMP6s and GCaMP6f. Fast (solid cyan) and slow (dashed cyan) exponents are shown for the FGCaMP7 indicator at 400 nm excitation. Data were fitted to the equation $k_{obs} = k_{on} \times [Ca^{2+}]^n + k_{off}$. (**i**) Relative contribution of monoexponents $A_1/(A_1 + A_2)$ and $A_2/(A_1 + A_2)$ for the FGCaMP7 indicator at 400 nm excitation, where A_1 and A_2 are the pre-exponential factors in the association curve equation $\Delta Flu(t) = A_1 \times \exp(-k^{on}_{obs1} \times t) + A_2 \times \exp(-k^{on}_{obs2} \times t)$. (**j**) Calcium-dissociation kinetics for FGCaMP, FGCaMP7, GCaMP6s and GCaMP6f. Starting concentration of free Ca^{2+} was 1000 nM. Three replicates were averaged for analysis. Where denoted, whiskers correspond to SD errors.

The M13-like peptide is tightly bound to the complex CaM-4 Ca^{2+}. The CaM/M13 pair is linked to the cpEGFP moiety by two linkers (with a length of 3 and 2 amino acids, respectively) with chromophore partially exposed from the cpEGFP barrel (see Figure 1a, Figure S1 and S2).

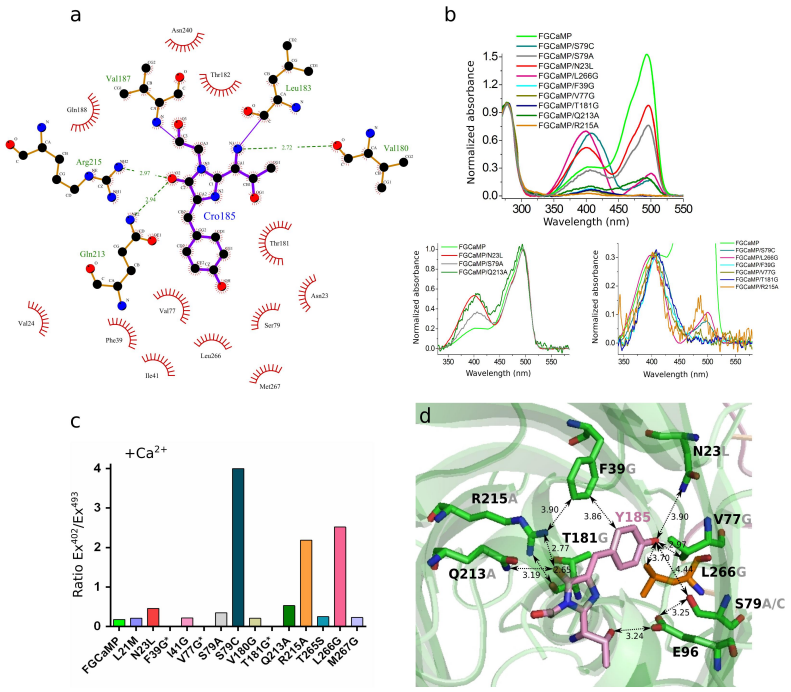

Figure S2. Absorbance ratio for two forms of calcium indicator FGCaMP and its mutants. **(a)** The immediate surroundings of the chromophore. **(b, top)** Absorbance for FGCaMP and its nine mutants in Ca^{2+}-saturated state. Absorbance spectra are presented only for nine FGCaMP mutants with substantial change in the Abs^{402}/Abs^{493} ratio. Absorbance at 280 nm is normalized to 1. **(b, bottom left)** Absorbance spectra of FGCaMP mutants with dominant 493 nm absorbing form. Absorbance at 493 nm is normalized to 1. **(b, bottom right)** Absorbance spectra of FGCaMP mutants with dominant 402-nm absorbing form. Absorbance at 402 nm is normalized to 0.3. **(c)** Abs^{402}/Abs^{493} ratios are presented for all 14 FGCaMP mutants in 13 amino acid positions in Ca^{2+}-saturated state. Mutants with absent anionic 493 nm absorbing form are marked with asterisk. **(d)** Chromophore and eight nearby mutated amino acid residues of the FGCaMP indicator (PDB 6XU4). Only residues leading to substantial change in the Abs^{402}/Abs^{493} ratio are shown. Distances between mutated amino acids and chromophore are indicated above black arrows. Amino acid codes and numberings in initial FGCaMP are in black; mutation codes are in light grey. Chromophore residue, residues from fluorescent domain and linker are shown in pink, green and orange, respectively.

Synthetic GFP chromophore in neutral water solution has an absorption maximum at 370 nm and an absorption maximum at 470–500 nm in GFP-like fluorescent proteins has been observed due to the surrounding amino acid environment inside the protein [3][4]. We have previously shown that the ratiometric indicator FGCaMP has one main absorption peak at 493 nm in Ca^{2+}-bound state and one absorption peak at 402 nm in Ca^{2+}-free state (Table 1 and [1]). To understand which amino acid residues participate in the stabilization of the FGCaMP anionic form with an absorption maximum at 493 nm in Ca^{2+}-bound state, we analyzed the amino acid environment of the FGCaMP chromophore using the obtained FGCaMP crystal structure and studied the impacts of the suggested point mutations on the FGCaMP absorption spectrum. According to the structural data analysis, we mutated the amino acid residues of FGCaMP located on the β-barrel of cpEGFP (N23, F39, I41, V77, S79, V180, T181, Q213, R215), on CaM (M267), and on linker 2 (L266), which were within 3.4–4.8 Å of the chromophore and which potentially affect the ratio of protonated and anionic forms of FGCaMP (Figure S2a). Two additional positions of the linkers (L21 and T265) were also mutated but were located far from the chromophore surroundings. Substitutions to small, non-polar residues (F39G, I41G, V77G, S79A, V180G, T181G, Q213A, R215A, L266G, and M267G) or to structurally similar non-polar or polar residues (L21M, N23L, S79C, and T265S) were made. Mutants were expressed in *Escherichia coli* and proteins were extracted from bacteria and dialyzed against buffer containing 10 mM $CaCl_2$. To determine which substitutions stabilized the 493 nm-absorbing form, the ratios of forms with absorption maxima at 402 and 493 nm (Abs^{402}/Abs^{493}) were estimated.

Table 1. In vitro characterization of FGCaMP7 indicator.

Properties	**Proteins**			
	FGCaMP		**FGCaMP7**	
	Apo	**Sat**	**Apo**	**Sat**
Absorbance maximum (nm)	**402**	**493**	**400**	**498**
Emission maximum (nm)	**516**		**516**	

Properties		Proteins			
		FGCaMP		FGCaMP7	
		Apo	Sat	Apo	Sat
Quantum yield [a]		0.48 ± 0.02	0.46 ± 0.01	0.40 ± 0.02	0.55 ± 0.04
ε ($mM^{-1}cm^{-1}$) [b]		55 ± 5	106 ± 20	82 ± 11	103 ± 14
Brightness (%) [c]		100	100	123	116
Fluorescence contrast (fold)	Ex 400/402	6.9 ± 0.5		9.3 ± 0.3	
	Ex 498/493	14.7 ± 0.6		38.4 ± 0.9	
Fluorescence contrast with 1 mM $MgCl_2$ (fold)	Ex 400/402	7.1 ± 0.2		10.1 ± 1.0	
	Ex 498/493	15.3 ± 0.5		32.7 ± 1.5	
pK_a (Ex 400) [d]		6.56 ± 0.03	7.0 ± 0.6	6.63 ± 0.20	6.00 ± 0.20
pK_a (Ex 498) [d]		6.2 ± 0.2	7.33 ± 0.07	5.28 ± 0.10; 7.81 ± 0.10	6.87 ± 0.01
K_d (nM) [e]	Ex 400	276 ± 9 (*n* = 2.8 ± 0.3)		130 ± 10 (*n* = 2.7 ± 0.1)	
	Ex 498	273 ± 7 (*n* = 3.5 ± 0.3) 4700 ± 200 (*n* = 1.9 ± 0.2)		160 ± 10 (*n* = 2.6 ± 0.2)	
K_d (nM) with 1 mM $MgCl_2$ [e]	Ex 400	460 ± 60 (*n* = 2.3 ± 0.6)		230 ± 5 (*n* = 2.2 ± 0.1)	
	Ex 498	460 ± 40 (*n* = 2.8 ± 0.4) 4400 ± 800 (*n* = 1.9 ± 0.2)		240 ± 6 (*n* = 2.3 ± 0.2)	
k_{obs} (s^{-1}) (300 nM Ca^{2+}) [f]	Ex 400	0.37 ± 0.01		0.60 ± 0.01	
	Ex 498	0.35 ± 0.01		0.42 ± 0.01	
$t_{1/2}^{off}$ (s) [g]	Ex 400	1.2 ± 0.1		1.5 ± 0.1	
	Ex 498	1.4 ± 0.1		1.34 ± 0.02	
Protein state		monomer		monomer	
Maturation half-time (min) [h]		ND	27 ± 4	ND	ND
Photobleaching half-time (sec) [i]		54 ± 9	260 ± 40	462 ± 126	464 ± 97

First, we estimated the impacts of the introduced mutations on spectral characteristics and the Abs^{402}/Abs^{493} absorption ratio. The absorption peaks of protonated/anionic forms for FGCaMP/S79C, FGCaMP/L266G, and FGCaMP/R215A mutants in Ca^{2+}-saturated state were observed at 408/498 nm, 398/500 nm, and 403/485 nm, respectively; while, for other mutants, absorbance peaks for both forms were around 405/490 nm, with a slight shift in the range of 3 nm (Figure S2b). The Abs^{402}/Abs^{493} absorption ratios were changed to the greatest extent for three FGCaMP mutants—FGCaMP/S79C, FGCaMP/L266G, and FGCaMP/R215A—and were 22-, 16-, and 12-fold higher, compared to the FGCaMP indicator, respectively (Figure S2b,c). The Q213A, N23L, and S79A substitutions had Abs^{402}/Abs^{493} ratios increased by 2.9-, 3.0-, and 1.9-fold, respectively, compared to the respective ratio for FGCaMP. In FGCaMP/F39G, FGCaMP/V77G, and FGCaMP/T181G mutants, the formation of the anionic 493 nm-absorbing form was blocked, making it impossible to evaluate the absorbance ratio (Figure S2b,c). Five other substitutions (L21M, I41G, V180G, T265S, and M267G) did not change the absorbance ratio significantly, compared to the ratio for the control FGCaMP (Figure S2c). Thus, according to the impacts of FGCaMP mutations on the Abs^{402}/Abs^{493} ratios, they were divided into four groups: mutations significantly increasing the Abs^{402}/Abs^{493} ratio (S79C, R215A, and L266G), mutations moderately increasing the Abs^{402}/Abs^{493} ratio (N23L, S79A, and Q213A), mutations with absorption only at 402 nm (F39G, V77G, and T181G), and mutations with no effect on the Abs^{402}/Abs^{493} ratio (L21M, I41G, V180G, T265S, and M267G).

Next, we attempted to explain the observed impacts of the mutations with a pronounced effect on the FGCaMP absorption. Among the eight amino acid residues which affected the Abs^{402}/Abs^{493} ratio, S79 (S205 in GFP) was located at the largest distance from the chromophore (4.44 Å) (Figure S2d)but had the most pronounced impact on the Abs^{402}/Abs^{493} ratio (Figure S2c). In the case of the wild-type GFP, S205 is known to participate in the hydrogen bonding network from E222 (E96 in FGCaMP, see Figure S2d) through the water molecule to the phenolic hydroxyl group of the

chromophore, thus maintaining the protonated form of GFP [5]. As the S–H group is more acidic than O–H [6], we suggest that cysteine in position 79 protonates to the hydroxyl of the FGCaMP chromophore and stabilizes the protonated state of the chromophore. S79A mutation also stabilized the protonated form of the chromophore, perhaps due to the small size of the alanine residue which increased the solvent accessibility of the chromophore, but with a more moderate effect on the Abs^{402}/Abs^{493} ratio compared to the S79C mutation (Figure S2c).

The L266 residue, on the linker between cpEGFP and CaM, was at a distance of 3.70 Å from the phenolic hydroxyl of the chromophore (Figure S2d). Its substitution to the small non-polar glycine changed the Abs^{402}/Abs^{493} ratio 16-fold, probably as a consequence of the decreased hydrophobic core near the chromophore, which may have led to an increase in chromophore solution accessibility and, subsequently, to stabilization of protonated form of the FGCaMP/L266G mutant (Figure S2b,c).

Another mutation, R215A (R96 in GFP), also increased the Abs^{402}/Abs^{493} ratio, indicating that this position was important for stabilization of the FGCaMP anionic form. R215 provided a positive charge at 2.77 Å distance from the carbonyl oxygen of imidazolinone (Figure S2d), which may stabilize the anionic form of FGCaMP. This hypothesis is also supported by the data obtained previously for the GFP protein, showing that R96 stabilizes the anionic form of the mature chromophore [7]. It has been described earlier that the R96 position in GFP is important for chromophore cyclization and the red-shift in the excitation maximum of intact protein (compared to the denatured one) and the R96A mutation in GFP blue-shift excitation maximum of the protein from 489 to 468 nm [8]. Accordingly, in the case of FGCaMP, the R215A mutation also blue-shifted the excitation maximum of the anionic form from 493 to 485 nm (Figure S2b).

The Q213A mutation (position Q94 in GFP) slightly increased the Abs^{402}/Abs^{493} ratio, probably due to the removal of hydrogen bond (H-bond) donors/acceptors near the imidazolinone ring of the chromophore (Figure S2c,d). Therefore, the H-bond donor/acceptors in position 213 and positive charge in position R215 are important for stabilization of the FGCaMP anionic form in Ca^{2+}-saturated state, due to the support of the polar chromophore environment; similar to that in GFP [9]. T181 (T62 in GFP) and Q213 residues in FGCaMP create a polar environment (Figure S2d), stabilizing the anionic 493 nm-absorbing form of FGCaMP, as has been shown earlier for GFP [9][10]. Probably for this reason, the T181G mutation lacked a 493 nm absorbing form and showed only a protonated 402 nm absorbing form (Figure S2b). The R215A and T181G mutations also disturbed protein folding with efficient chromophore formation. The mutation of N23 to non-polar leucine, at a 3.90 Å distance from the chromophore (Figure S2d), led to a moderate increase in the Abs^{402}/Abs^{493} ratio; probably due to destabilization of the anionic form of the FGCaMP chromophore via deletion of the direct H-bond with the hydroxyl of the phenolic group of the chromophore (Figure S2c).

The F39G mutation blocked formation of the anionic form of the FGCaMP indicator (Figure S2b,c). F39 (F165 in GFP) seemed to create a non-polar environment around the chromophore and hold the polar core (composed of R215 and Q213 residues) around the chromophore (Figure S2d), as has been earlier predicted for GFP [9]. Furthermore, the F39 residue may provide hydrophobicity and participate in stacking interactions with the chromophore, thus stabilizing the anionic form of FGCaMP.

Threonine 203 in GFP forms an H-bond with the phenolic hydroxyl of the chromophore and, so, the T203I mutation led to the absence of the 475 nm absorbing form in the wild-type GFP [10]. The T203V substitution, which cannot form an H-bond with the phenolic hydroxyl of the chromophore, is also known to destabilize the anionic form of GFP [11]. However, even though FGCaMP has valine in the 77 position (analogous to the 203 position in GFP), the anionic 493 nm absorbing form in FGCaMP dominated over the protonated 402 nm absorbing one (Figure S2b). We suggest that, in the case of FGCaMP, the V77 residue forms a hydrophobic core around the chromophore together with other non-polar amino acids; this core may be important for the stabilization of the FGCaMP anionic form. V77G mutation led to the disappearance of anionic 493 nm absorbing form of FGCaMP, probably due to a reduction of the size of hydrophobic core (Figure S2b-d) and increasing solvent accessibility for the chromophore. Both F39G and V77G mutations impaired FGCaMP folding with efficient chromophore formation (Figure S2b).

Hence, of the 12 mutants of the FGCaMP indicator near the chromophore (i.e., within 3.4–4.8 Å) plus the two mutants with substitutions in linker positions 9–10 Å far from the chromophore, we found three mutations (S79C, R215A, and L266G) which substantially affected the absorption ratio for both protonated and anionic forms of the FGCaMP indicator in Ca^{2+}-saturated state. Three other mutations (F39G, V77G, and T181G) blocked the formation of anionic form of FGCaMP. Hence, the residues in the positions 39, 77, 79, 181, 215, and 266 participate in the stabilization of the anionic form of the FGCaMP indicator. We suggest that the hydrophobic core around chromophore is important for the stabilization of anionic form. Namely, the mutations L266G, F39G, and V77G reduced (or fully eliminated) formation of anionic form, probably by decreasing the hydrophobic core around chromophore (Figure S2b-d). The polar amino acids near the hydroxyl of a

phenolic ring of the chromophore (S79 and N23) or close to the carbonyl group of imidazolinone of the chromophore (Q213A, R215A, and T181G) also substantially contributed to the stabilization of the anionic form of FGCaMP (Figure S2b-d).

2. Development of Improved Version of GECI Based on Fungi Calcium-Binding Parts

Introducing the mutations described above within the surroundings of the FGCaMP chromophore, we tried to find variants with properties outperforming the initial FGCaMP indicator. To that end, we conducted a contrast analysis of purified mutants for both 402- and 493 nm- absorbing forms (Table S2). In the case of 493 nm-absorbing forms, nine mutants had contrasts 1.4–11.3-fold smaller than the contrast of FGCaMP. FGCaMP/L21M, FGCaMP/N23L, FGCaMP/V180G, FGCaMP/Q213A, and FGCaMP/T265S mutants had similar contrasts and mutant FGCaMP/S79A had a contrast 1.8-fold higher than the contrast of FGCaMP, but the contrast of its 402-nm absorbing form was 23-fold smaller than the contrast of FGCaMP. The 402-nm absorbing forms of all other mutants had contrasts 1.8–9.9-fold smaller than the contrast of the respective form of FGCaMP (Table S2). Hence, none of the structurally guided or rationally introduced mutations could enhance the properties of the FGCaMP indicator at no cost for the other characteristics.

Table S2. In vitro contrasts of FGCaMP mutants

Protein	Contrast for 402 nm-form	Contrast for 493 nm-form
FGCaMP	6.9 ± 0.5	14.7 ± 0.6
FGCaMP/L21M	2.9 ± 0.3	17.6 ± 1.2
FGCaMP/N23L	1.6 ± 0.2	17.2 ± 7.8
FGCaMP/F39G*	1.0 ± 0.1	1.3 ± 0.1
FGCaMP/I41G	2.1 ± 0.3	3.3 ± 0.3
FGCaMP/V77G*	1.5 ± 0.2	1.5 ± 0.2
FGCaMP/S79A	0.30 ± 0.05	27.0 ± 1.4
FGCaMP/S79C	0.7 ± 0.1	6.2 ± 0.3
FGCaMP/V180G	2.2 ± 0.1	11.9 ± 0.4
FGCaMP/T181G*	0.9 ± 0.1	1.5 ± 0.2
FGCaMP/Q213A	3.9 ± 0.5	12.6 ± 2.7
FGCaMP/R215A*	0.8 ± 0.1	1.6 ± 0.2
FGCaMP/T265S	3.4 ± 0.4	14.1 ± 2.9
FGCaMP/L266G	1.9 ± 0.2	1.9 ± 0.3
FGCaMP/M267G	1.5 ± 0.1	10.7 ± 1.3

* Mutations that impaired FGCaMP folding.

As we were not able to improve the contrast of the FGCaMP indicator by introducing mutations in the surroundings near its chromophore, we decided to use the strategy of random mutagenesis and screening for further indicator evolution. The main drawback of FGCaMP is its bi-phasic Ca^{2+}-binding curve with high- (K_{d1}) and low-affinity (K_{d2}) calcium components at 493 nm excitation, which ensures a non-linear response of the indicator with elevated of calcium ion concentration, potentially substantially reducing the fluorescence response of the indicator at low calcium ion concentrations in vivo. To further improve the properties of the FGCaMP indicator (Figure 1a, top), we chose mutants which we developed previously by directed mutagenesis of CaM/M13-peptide [1] with a mainly mono-phasic calcium-binding curve as a consequence of decreased contrast of the second (K_{d2}) component at 493 nm excitation. These mutants had widely varying K_ds values (FGCaMP2/T28D, K_{d1} 433 nM at 493 nm; FGCaMP3, K_{d1} 208 nM at 493 nm; FGCaMP4, K_{d1} 98 nM at 493 nm; Table S3, Figure S3). Based on these mutants, we generated three random libraries. We analyzed mutants from these libraries and collected clones with the highest brightness and K_{d1} contrast at both 402 nm and 493 nm excitation and decreased K_{d2} contrast at 493 nm excitation, using two-step screening strategy in *E. coli* cells [1][12][13].

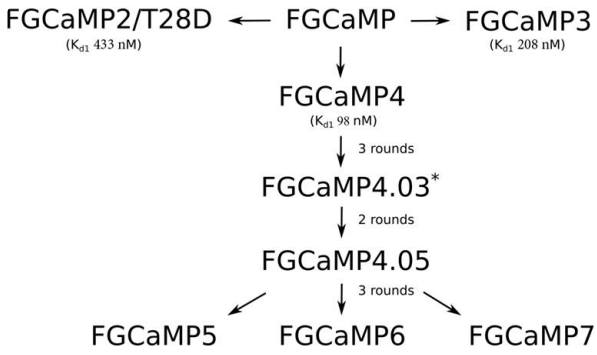

Figure S3. Genealogy of FGCaMP variants.
* Beginning from the third round mutants have monophasic calcium-binding curve with single dissociation constant (K_d).

Table S3. Mutations in FGCaMP variants described in this work

Protein	Mutations relative to FGCaMP*
FGCaMP2	**N327D/D345Y/T346R/N364D**
FGCaMP3	**N327D/D345Y/T346R/N364D/S368D**
FGCaMP4	**T3L/H5K/N327D/D345Y/T346R/N364D/S368D**
FGCaMP4.03	**T3L/H5K/L21M/D221G/N327D/K342E/D345Y/T346R/S348T/A355V/N364D/S368D**
FGCaMP4.05	**T3L/H5K/L21M/K122R/F218L/D221G/D325G/N326S/N327D/K342E/D345Y/ T346R/S348T/A355V/N364D/S368D**
FGCaMP5	**T3L/H5K/N5I/L21M/D47G/K122R/F218L/D221G/T265S/D325G/N326S/N327D/ K342E/D345Y/T346R/S348T/A355V/N364D/S368D**
FGCaMP6	**T3L/H5K/L21M/D47G/K122R/T162A/F218L/D221G/T265S/T272A/D325G/ N326S/N327D/K342E/D345Y/T346R/S348T/A355V/N364D/S368D**
FGCaMP7	**T3L/H5K/L21M/D47G/K88Q/K122R/F218L/D221G/T265S/D325G/N326S/N327D/K342E/D345Y/ T346R/S348T/A355V/N364D/S368D**

* Substitution number follows that of FGCaMP sequence. Unique mutations for the novel FGCaMP5, FGCaMP6, and FGCaMP7
variants are bold.

Clones selected after the screening of libraries based on FGCaMP2/T28D and FGCaMP3 had K_{d1} around 2.5 and 1.5 μM, respectively, which are not appropriate for the monitoring of calcium neuronal activity (K_d of 200 nM is considered optimal for neurons). The most promising variants were found in the library based on FGCaMP4 and, therefore, we focused on the directed evolution of this variant. The FGCaMP4 library was analyzed using a two-step screening strategy in each round of random mutagenesis. During the first step, we performed imaging of the indicator's library targeted to the *E. coli* periplasm on Petri dishes and selected clones with the highest fluorescence ratio before and after treatment, using a buffer that contained ethylenediaminetetraacetic acid (EDTA) using 405/40BP and 480/40BP nm excitation filters and 510LP and 535/40BP nm emission filters, respectively. During the second step, the selected clones were analyzed in bacterial extracts in B-Per reagent. To eliminate the second component with low affinity to calcium ions, we selected proteins with minimal fluorescence ratio at 10 mM Ca-EGTA ([Ca^{2+} = 39 μM]) to 9 mM Ca-EGTA ([Ca^{2+} = 1.35 μM]) at 490 nm excitation. As a result, after three rounds of mutagenesis, we found an FGCaMP4.03 clone (Table S3, Figure S3) with monophasic Ca^{2+}-binding curve and 300 nM affinity to calcium ions in the presence of 1 mM $MgCl_2$ and fluorescence contrast 1.6-fold higher than the contrast of original FGCaMP at 493 nm in vitro (23.3 ± 1.2 for FGCaMP4.03 vs. 14.7 ± 0.6 for FGCaMP). The selected mutant had approximately 2-fold lower brightness, compared to the original FGCaMP, and slow association/dissociation kinetics in spontaneously active cultured neurons. Hence, we decided to further improve the selected FGCaMP4 variant.

After eight rounds of the random mutagenesis and screening described above, we found three promising variants—named FGCaMP5, FGCaMP6, and FGCaMP7—which preserved the ratiometric response of the parental FGCaMP to calcium ions and had in vitro fluorescence contrasts to 10 mM $CaCl_2$ addition of 8.0-, 9.0-, and 10.1-fold at 400 nm excitation and 17.6-, 33.0-, and 32.7-fold at 498 nm excitation, respectively (Table S4).

Table S4. In vitro characterization of FGCaMP5, FGCaMP6, and FGCaMP7 indicators

		Proteins					
Properties		FGCaMP7		FGCaMP5		FGCaMP6	
		apo	sat	apo	sat	apo	sat
Absorbance maximum (nm)		400	498	400	497	400	496
Emission maximum (nm)		516		516		516	
Quantum yield [a]		0.4 ± 0.02	0.55 ± 0.04	0.57 ± 0.04	0.56 ± 0.05	0.32 ± 0.01	0.53 ± 0.04
e ($mM^{-1}cm^{-1}$) [b]		82 ± 11	103 ± 14	77 ± 13	119 ± 16	54 ± 10	104 ± 11
Brightness (%) [c]		123	116	166	137	65	113
Fluorescence contrast (fold) with 1 mM $MgCl_2$	Ex 400	10.1 ± 1.0		8.0 ± 0.4		9.0 ± 0.1	
	Ex 498	32.7 ± 1.5		17.6 ± 1.1		33.0 ± 0.3	

	Ex 400	6.63 ± 0.20	6.00 ± 0.20	7.01 ± 0.03	5.75 ± 0.15	6.84 ± 0.02	5.57 ± 0.04
pKa [d]	Ex 498	5.28 ± 0.10 7.81 ± 0.10	6.87 ± 0.01	6.44 ± 0.09	6.86 ± 0.03	6.80 ± 0.01	6.88 ± 0.03
K_d (nM) with 1 mM $MgCl_2$ [e]	Ex 400	230 ± 5 (n = 2.2 ± 0.1)		87 ± 1 (n = 1.6 ± 0.1)		240 ± 60 (n = 1.8 ± 0.1)	
	Ex 498	240 ± 6 (n = 2.3 ± 0.2)		98 ± 3 (n = 1.8 ± 0.2)		350 ± 13 (n = 1.8 ± 0.1)	
k_{obs} (s^{-1}) (300 nM Ca^{2+}) [f]	Ex 400	0.60 ± 0.01		6.3 ± 0.4; 1.01 ± 0.01		5.2 ± 0.1; 0.80 ± 0.01	
	Ex 498	0.42 ± 0.01		0.81 ± 0.01		0.52 ± 0.02	
$t_{1/2}^{off}$ (s) [g]	Ex 400	1.5 ± 0.1		2.2 ± 0.1		1.2 ± 0.1	
	Ex 498	1.34 ± 0.02		2.01 ± 0.02		0.97 ± 0.02	

[a] mEGFP (QY = 0.61[1]) and mTagBFP2 (QY = 0.64 [2]) were used as reference standards for 496–498 and 400 nm absorbing states, respectively.

[b] Extinction coefficient was determined by alkaline denaturation.

[c] Brightness normalized to brightness of FGCaMP indicator.

[d] p*K*a values were determined according to pH dependence of fluorescence.

[e] Experimental data was fitted to Hill equation. Hill coefficients are shown in square brackets.
K_d for GCaMP6s 144 ± 9 nM (4.0 ± 0.6); in the presence of 1 mM $MgCl_2$ K_d for GCaMP6s 217 ± 16 nM (4.0 ± 0.6).

[f] Observed Ca^{2+}-associated rate constants were determined from associated curves in the presence of 1 mM $MgCl_2$.
k_{obs} for GCaMP6s is 0.49 ± 0.01 s^{-1}, k_{obs} for GCaMP6f is 1.28 ± 0.01 s^{-1}.

[g] $t_{1/2}^{off}$ values were determined from the dissociation kinetics curves in the presence of 1 mM $MgCl_2$.
$t_{1/2}^{off}$ for GCaMP6s is 1.01 ± 0.06 s; $t_{1/2}^{off}$ for GCaMP6f is 0.37 ± 0.04 s.

FGCaMP5 and FGCaMP7 had 19 amino acid substitutions relative to the original FGCaMP, and FGCaMP6 had 20 amino acid substitutions (Figure S4 and S5). Among these mutations, 13 or 12 were located in the *A. niger/A. fumigatus*-derived M13-peptide/CaM of FGCaMP5 and FGCaMP6 or FGCaMP7, respectively; four or five mutations were located in the cpEGFP-based fluorescent domain of FGCaMP5 or FGCaMP6 and FGCaMP7, respectively; and two mutations were located in linkers between the Ca^{2+}-binding and fluorescent domains (Figure S4 and S5).

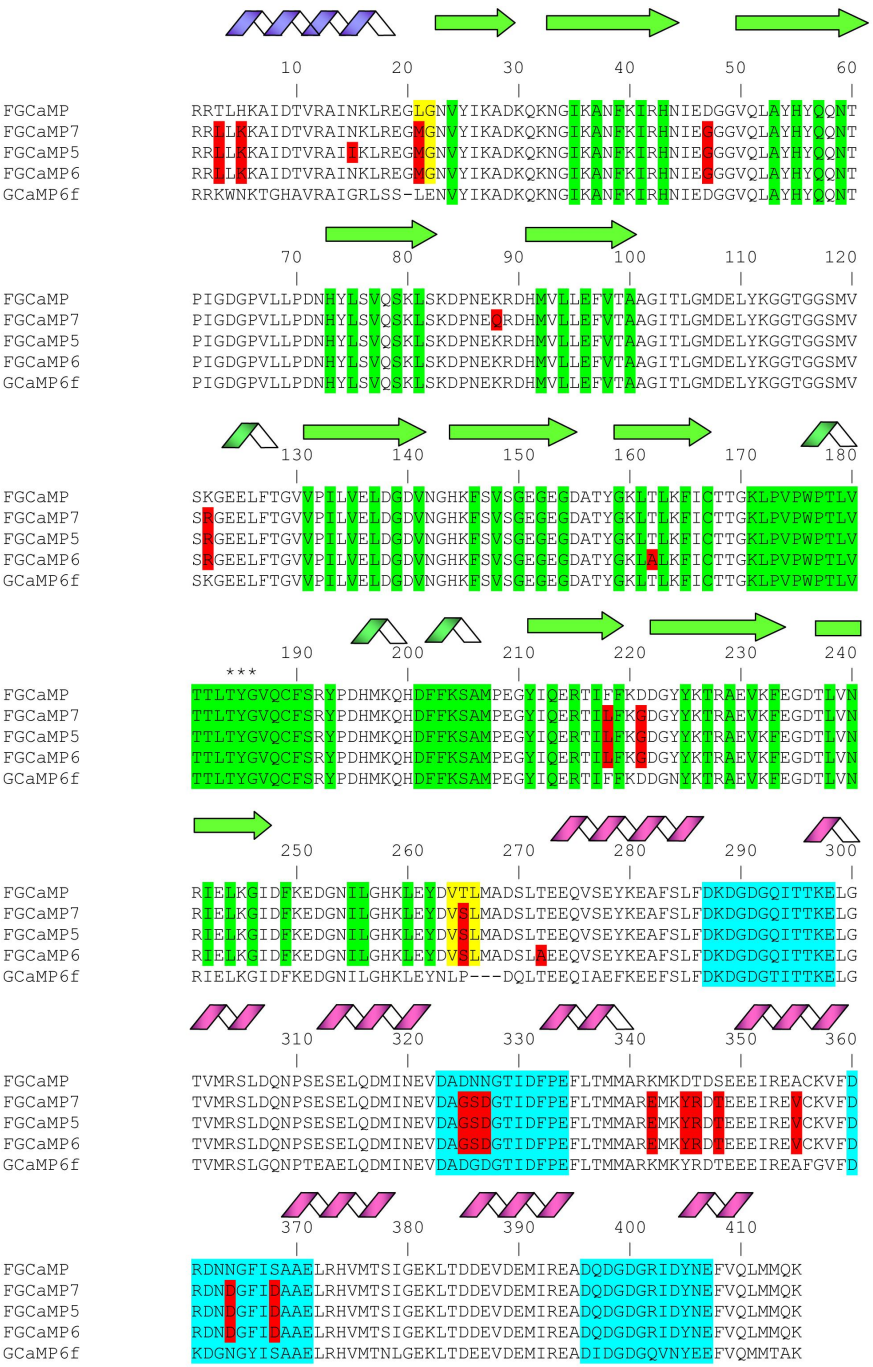

Figure S4. Alignment of the amino acid sequences for FGCaMP, FGCaMP5, FGCaMP6, FGCaMP7, and GCaMP6f calcium indicators. Alignment number follows that of FGCaMP. Residues of fluorescent part buried in β-barrel are highlighted with green. Residues that are forming chromophore are marked with asterisks. Calcium-binding EF1–EF4 hands are highlighted with cyan. Linkers between fluorescent and calcium-binding parts are highlighted with yellow. Mutations in FGCaMP variants relative to the original FGCaMP are highlighted with red. Secondary structure of FGCaMP is presented on top.

All mutations located in fluorescent domain were external to the β-barrel of GFP and were not likely to affect chromophore properties (Figure S5). All three chosen indicators had five mutations in the Ca^{2+}-binding EF-hands: three mutations in EF2, and two in EF3. N327D, N364D, and S368D substitutions were previously introduced by site-directed mutagenesis; these mutations have been shown to decrease the K_d value of high-affinity components for the FGCaMP indicator [1]. FGCaMP5 had one unique N15I mutation in the M13-peptide, FGCaMP6 had two unique T162A and T272A substitutions, and FGCaMP7 had one unique K88Q mutation in the fluorescent domain (Table S3 and Figure S4). The location of the FGCaMP7 mutations along the gene of FGCaMP are presented schematically in Figure 1a (bottom).

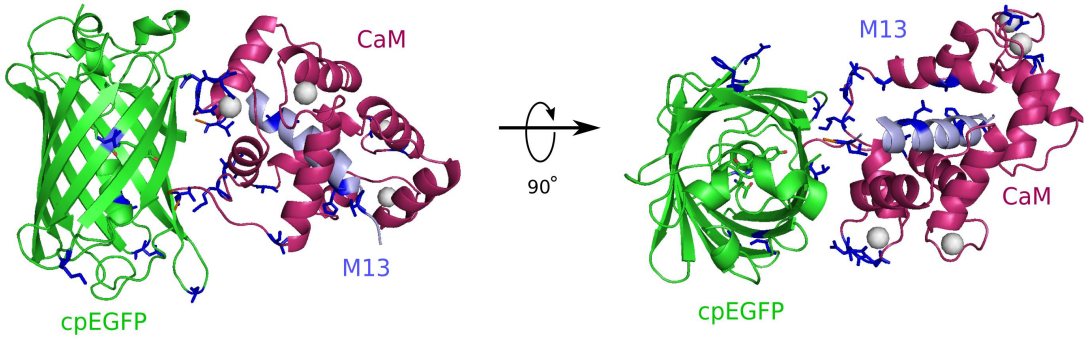

Figure S5. Cartoon representation of FGCaMP calcium indicator with mutations from FGCaMP5, FGCaMP6, and FGCaMP7 variants. Orthogonal views of the structure of FGCaMP indicator in Ca^{2+}-bound state (PDB 6XU4). β-barrel of cpEGFP is shown as a green cylinder, Ca^{2+} ions are shown as grey spheres, M13-peptide and CaM are shown in purple and light blue, respectively. Positions of FGCaMP5, FGCaMP6, and FGCaMP7 mutations relative to FGCaMP structure are depicted as blue sticks.

3. In Vitro Properties of Improved Purified FGCaMP Variants

The key in vitro characteristics of the improved variants of the FGCaMP indicator were determined and are summarized in Table 1 and Table S4. Spectroscopic data showed that FGCaMP5, FGCaMP6, and FGCaMP7 exhibited absorbance peaks at 400 nm in Ca^{2+}-free state and 496–498 nm in Ca^{2+}-saturated state (Table S4 and Figure 1b,c). When excited at 400 and 496–498 nm, the FGCaMP variants fluoresced at one emission peak at 516 nm (Table S4and Figure 1b,c). All three FGCaMP variants had slightly (3–5 nm) smaller Stokes shift, compared to the original FGCaMP. The 400 and 496–498 nm absorption maxima can be attributed to the protonated and anionic forms of GFP chromophore, respectively, similar to the original FGCaMP indicator [1][3]. In Ca^{2+}-saturated states, the brightness of FGCaMP5, FGCaMP6, and FGCaMP7 were 1.37-, 1.13-, and 1.16-fold higher than the brightness of the FGCaMP anionic form, respectively (Table S4). In Ca^{2+}-free states, the brightness of FGCaMP5 and FGCaMP7 were 1.66- and 1.23-fold higher than that of FGCaMP, respectively; while the 400-nm absorbing form of FGCaMP6 had only 65% brightness of the original FGCaMP indicator (Table S4).

Upon calcium ion binding, the maximal fluorescence of FGCaMP7 and FGCaMP6 in the presence of 1 mM $MgCl_2$ (equivalent to 0.58–1 mM free Mg^{2+} ion concentration, resembling that of 0.5–1.5 mM in the cytosol of mammalian cells [14][15]) showed 10.1- and 9.0-fold decreases and 32.7- and 33.0-fold increases at 400 and 496–498 nm excitation, respectively (Table 1 and Table S4). These contrasts were 1.4- and 1.3-fold and 2.1- and 2.2-fold higher than the fluorescence contrasts of the respective forms of the original FGCaMP indicator. The fluorescence contrasts for the FGCaMP5 mutant (8.0 ± 0.4- and 17.6 ± 1.1-fold at 400 and 498 nm, respectively) were comparable to those of FGCaMP (7.1 ± 0.2- and 15.3 ± 0.5-fold at 402 and 493 nm, respectively). Thus, the selected FGCaMP variants are excitation-ratiometric calcium indicators with 140–330-fold maximal fluorescence contrast ratio change upon calcium ion binding. The maximal fluorescence contrast ratio for FGCaMP7 (330-fold) was 3.0-fold higher than that for FGCaMP (109-fold) in the presence of 1 mM $MgCl_2$. Recently, another ratiometric calcium indicator series, Y-GECO2s, has been published with maximal contrasts ratio 1.1–2.3-fold higher than the contrast ratio for the FGCaMP7 indicator, which demonstrated the largest contrast among the studied FGCaMPs [16]. However, Y-GECO2s still suffer from low extinction coefficients and its molecular brightness at 412 and 522 nm excitation were 2.8–3.3-fold and 3.1–3.5-fold lower than the brightness of the FGCaMP indicators at 400 and 498 nm excitation, respectively [16]. Hence, enhanced FGCaMPs are the GECIs of choice among the currently available ratiometric indicators, in terms of high dynamic range and molecular brightness.

We next assessed the affinity of FGCaMP variants to Ca^{2+} ions. According to equilibrium binding titration curves, FGCaMP demonstrates bi-phasic Ca^{2+} binding in the range of 0–39 μM free Ca^{2+} at 493 nm excitation. Such bi-phasic Ca^{2+} binding of FGCaMP is a limitation, as it decreases the sensitivity of the indicator to low calcium ion concentration transients and violates its linear response at high calcium ion concentrations when expressed in neurons. In the presence of 1 mM $MgCl_2$, FGCaMP5, FGCaMP6, and FGCaMP7 demonstrated mono-phasic calcium titration curves with K_d values of 98 ± 3 nM, 350 ± 13 nM, and 240 ± 6 nM, respectively (Figure 1d and Figure S6a,b and Table 1 and Table S4). These values were 4.7-, 1.3-, and 1.9-fold lower than the K_d value for FGCaMP under the same conditions and were optimal for the monitoring of calcium concentration changes during neuronal activity, which typically varies from 50–100 nM at rest to 250–10,000 nM during activation in the cytosol of mammalian cells [17][18]. The high calcium affinity of the FGCaMP5 indicator is probably a result of the N15I substitution in the M13-peptide (Figure S4), which may strengthen its interactions

with the Ca^{2+}-binding domains of CaM. Indeed, N15I was a unique mutation among the FGCaMP5, FGCaMP6, and FGCaMP7 indicators; it has been previously shown that mutations in the M13-peptide remarkably affected the indicator's affinity to calcium ions [1]. According to the Hill coefficient values calculated by fitting the equilibrium titration curves to the Hill equation, the FGCaMP5, FGCaMP6, and FGCaMP7 indicators bound calcium ions with slightly less co-operativity, compared to the control FGCaMP and GCaMP6s indicators (Hill coefficients: 1.6–2.3 vs. 2.3–4.0; Table 1 and Table S4) [1] [19]. Hill coefficients in the range of 3–4 are common for many GECIs, which implies linear dependence of the ΔF/F response to changes in calcium concentration in a narrow calcium ion concentration range but with higher ΔF/F response. When the Hill coefficient is close to 1 or less (which is characteristic of most synthetic dyes), the ΔF/F dependence vs. [Ca^{2+}] is linear in a wider range of calcium ion concentrations [20][21]; however, this is at the expense of lower sensitivity. Hence, the enhanced versions of FGCaMP demonstrated advantageous mono-phasic fluorescence responses to calcium ions and had affinities to calcium ions appropriate for the monitoring of neuronal activity.

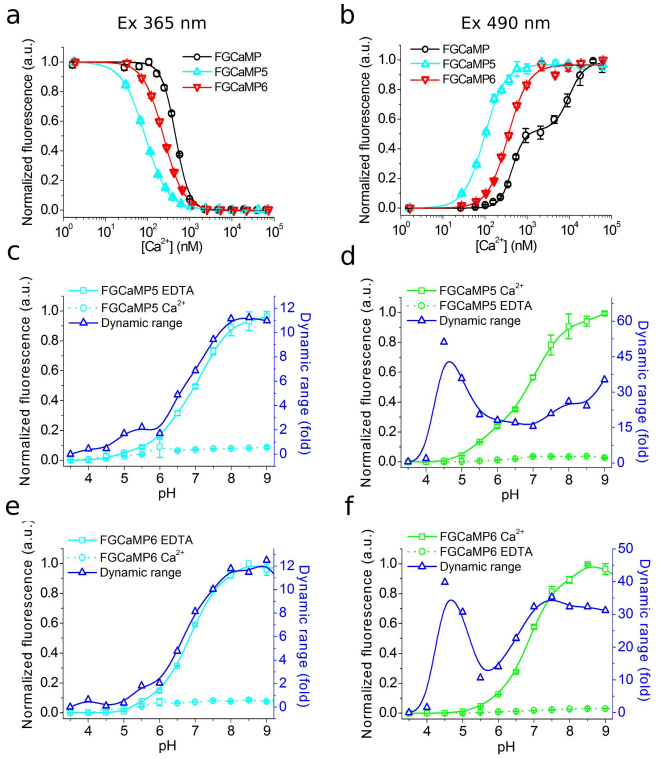

Figure S6. Calcium titration curves and pH dependences for FGCaMP5 and FGCaMP6. **(a)** Ca^{2+} titration curves for FGCaMP5 and FGCaMP6 at 365 nm excitation. **(b)** Ca^{2+} titration curves for FGCaMP5 and FGCaMP6 at 490 nm excitation. **(c)** Fluorescence of FGCaMP5 as a function of pH at 365 nm excitation. **(d)** Fluorescence of FGCaMP5 as a function of pH at 490 nm excitation. **(e)** Fluorescence of FGCaMP6 as a function of pH at 365 nm excitation. **(f)** Fluorescence of FGCaMP6 as a function of pH at 490 nm excitation.

Next, we characterized another important property of the improved FGCaMPs GECIs: their pH stability. According to fluorescence changes, the 400 nm absorbing form of FGCaMP7 exhibited a slight shift in pK_a value (from 6.63 to 6.00) after the addition of calcium ions (Figure 1e and Table 1). Upon Ca^{2+} binding, the pK_a values for the 498 absorbing form shifted from 5.28 and 7.81 to 6.87 (Figure 1f and Table 1). In the range of pH values of 7–8, which is typical in the cytosol of neurons [22], the changes of fluorescence intensity for the protonated form in Ca^{2+}-free state and anionic form in Ca^{2+}-saturated state were 25% and 36%, respectively, while the change of the dynamic ranges for both forms in the pH range 7–8 was minor—which is an advantage of FGCaMP7 (Figure 1e,f) the protonated forms of FGCaMP5 and FGCaMP6 showed larger shifts in pK_as, from 7.01 to 5.75 and from 6.84 to 5.57, respectively (Table S4), upon calcium-binding. The pK_a shifts of 496–497 nm absorbing forms for FGCaMP5 and FGCaMP6 were negligible (Table S4), considering that their anionic forms are more pH-stable than the respective form of FGCaMP7. In contrast to the FGCaMP7 indicator, the dynamic ranges for the protonated forms of FGCaMP5 and FGCaMP6 changed by about 25%–30% in the range of pH values 7–8 (Figure S6c,e). At the same time, changes in the dynamic ranges of anionic forms of FGCaMP5 and FGCaMP6 were negligible under the same conditions (Figure S6d,f). Hence, the fluorescence response of these FGCaMP variants may be affected by variations in pH.

Next, we assessed the photobleaching stability for the FGCaMP7 indicator, as the indicator combining high contrast and brightness for both forms and showing the best performance in neuronal cultures (see results below). Both protonated and anionic forms of FGCaMP7 were extremely photostable in vitro. Under a wide-field microscope equipped with a metal halide lamp and 470/40BP excitation filter, FGCaMP7 in Ca^{2+}-saturated state photobleached 2.7- and 1.8-fold slower than a control mEGFP protein and FGCaMP indicator in Ca^{2+}-saturated state. In the absence of Ca^{2+} ions, FGCaMP7

photobleached 8.7- and 8.6-fold slower than mTagBFP2 and FGCaMP as a result of illumination with 355 ± 25 nm light, respectively (Figure 1g and Table 1). Hence, both 400- and 498-forms of the FGCaMP7 indicator demonstrated photostability in vitro higher than the photostabilities of FGCaMP, mTagBFP2, and mEGFP proteins.

Both in the absence of Ca^{2+} and the presence of 1 mM Ca^{2+}, purified FGCaMP7 sensor eluted in size-exclusion chromatography as a monomer (Figure S7); note that monomeric proteins are usually preferable in terms of reduced cytotoxicity [23].

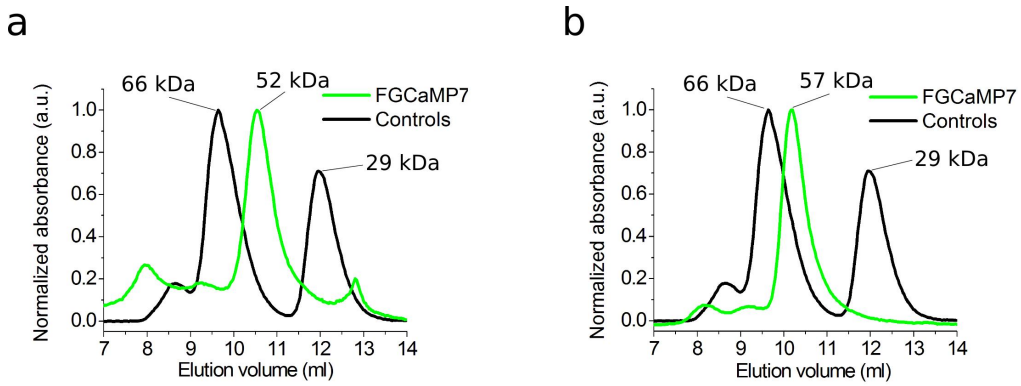

Figure S7. Size-exclusion chromatography for FGCaMP7 protein. **(a)** Fast protein liquid chromatography of FGCaMP7 in 20 mM Tris-HCl (pH 7.5), 100 mM NaCl buffer supplemented with 1 mM $CaCl_2$ or **(b)** in 20 mM Tris-HCl (pH 7.5), 200 mM NaCl buffer supplemented with 2 mM EDTA.

As fast Ca^{2+} association and dissociation kinetics are crucial for the resolution of neuronal dynamics, these kinetics were studied in the FGCaMP variants using stopped-flow fluorimetry. To investigate the association kinetics, we calculated the observed association rate constants (k_{obs}) at [Ca^{2+}] 300–1000 nM in the presence of 1 mM $MgCl_2$ by fitting the kinetic curves of FGCaMP5, FGCaMP6, and FGCaMP7 to double exponentials at 400 nm excitation, to a single exponential at 498 nm excitation, and the kinetic curves of the original FGCaMP to a single exponential at both excitation wavelengths (Figure S8a,b and Figure 1h). The contribution of exponent 1 at 400 nm excitation varied from 10% to 29% for FGCaMP5, from 34% to 49% for FGCaMP6, and from 0% to 35% for FGCaMP7 (Figure S8c and Figure 1i). According to the k_{obs} values obtained from the stopped-flow data, in the range of free Ca^{2+} concentrations 300–1000 nM, the FGCaMP5 indicator was the fastest among the FGCaMP mutants, which associated with calcium ions 1.1–1.9-fold faster than FGCaMP6 and FGCaMP7 at both 400 and 498 nm excitation (Figure S8b). At 300 nM calcium concentration, as observed in neurons at one action potential (AP), FGCaMP5 associated with calcium ions 2.1/1.7-fold or 2.7/2.3-fold faster than control GCaMP6s or progenitor FGCaMP at 400/498 nm excitation, respectively. At the same time, at 300 nM [Ca^{2+}] at 400 nm excitation, the FGCaMP7 indicator associated with calcium 2.1-fold slower than the fastest GCaMP6f indicator and 1.2- and 1.6-fold faster than GCaMP6s and FGCaMP (Figure 1h and Table S4). At 498 nm excitation, FGCaMP7 associated with calcium ions was 3.0-fold slower than GCaMP6f and had an association rate constant comparable to the respective constants for GCaMP6s and FGCaMP (Figure 1h and Table S4).

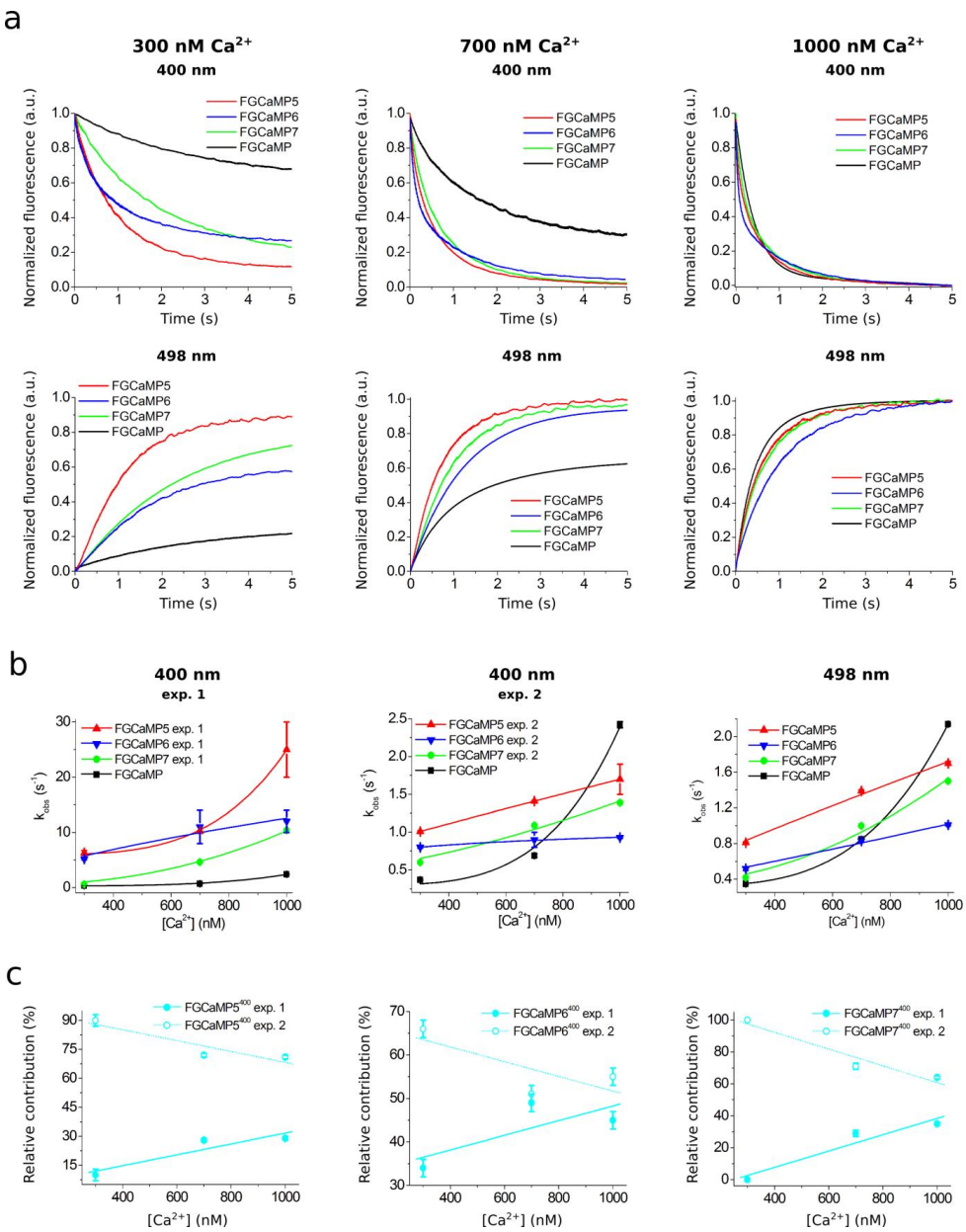

Figure S8. Calcium-association kinetics for the FGCaMP indicator series characterized by stopped-flow fluorimetry. **(a)** Calcium-association kinetics curves for FGCaMP, FGCaMP5, FGCaMP6, and FGCaMP7 GECIs at Ca^{2+} concentrations of 300 nM, 700 nM, and 1000 nM. Calcium-association curves are shown for both forms with maximum excitation at 400 and 498 nm. **(b)** Observed Ca^{2+}-association rate constants determined from association curves for FGCaMP, FGCaMP5, FGCaMP6, and FGCaMP7 GECIs. For the form with excitation maximum at 400 nm fast (exp. 1) and slow (exp. 2) exponents are shown. The data was fitted to the equation $k_{obs} = k_{on} \times [Ca^{2+}]^n + k_{off}$. **(c)** Relative contribution of monoexponents A1/(A1 + A2) and A2/(A1 + A2) for FGCaMP5, FGCaMP6, and FGCaMP7 GECIs at 400 nm excitation, where A1 and A2 are the pre-exponential factors in the association curve equation $\Delta Flu(t) = A1 \times \exp(-k^{on}_{obs1} \times t) + A2 \times \exp(-k^{on}_{obs2} \times t)$.

The dissociation half-time ($t_{1/2}^{off}$) of FGCaMP5 was 1.5–2.1-fold longer than the respective half-times for FGCaMP6 and FGCaMP7 (Table S4). The FGCaMP7 indicator at 400 nm excitation released calcium ions 1.5- and 1.3-fold slower than GCaMP6s and FGCaMP and 4.1-fold slower than GCaMP6f, respectively (Figure 1j and Table 1). At 498 nm excitation, the dissociation half-time of FGCaMP7 was similar to the dissociation half-time of FGCaMP and 1.3- or 3.6-fold longer than those obtained with GCaMP6s or GCaMP6f, respectively (Figure 1j and Table 1). Hence, enhanced FGCaMPs have fast association–dissociation kinetics for calcium ions, comparable to the kinetics of the standard GCaMP6s GECI, which demonstrates their suitability for the visualization of fast neuronal activity.

Thus, using directed molecular evolution, we substantially improved the new class of FGCaMP calcium indicators, based on Ca^{2+}-binding parts from fungi. As a result, for further characterization in HeLa cells and neuronal cultures, we selected three enhanced FGCaMPs variants which demonstrated a mono-phasic response to calcium ions, had different calcium affinities and dynamic ranges superior to that of FGCaMP, and which preserved the ratiometric phenotype of the original FGCaMP indicator.

4. Calcium-Dependent Response of Improved FGCaMP Indicators in HeLa Cells

To evaluate the behaviors of the enhanced FGCaMP indicators in live mammalian cells, we expressed FGCaMP5, FGCaMP6, and FGCaMP7, as well as control FGCaMP and GCaMP6s, in HeLa Kyoto cells together with a red reference R-GECO1 calcium indicator, and studied their response to ionomycin-induced elevation of calcium concentration in the cell cytosol [24]. After the addition of 2.5 μM ionomycin, we observed increases in red and green fluorescence when excited at 561 and 488 nm, respectively; green fluorescence at 405 nm excitation decreased (Figure 2 and Figure S9). The $\Delta F/F_0$ value for the fast calcium-associated FGCaMP5 normalized to $\Delta F/F_0$ of the R-GECO1 indicator was only 87 ± 25% at 488 nm excitation (Table 2). The mean normalized $\Delta F/F_0$ response for FGCaMP7 was 237 ± 81% from the R-GECO1 response, which was 2.1- and 1.5-fold higher than normalized responses for GCaMP6s ($p < 0.0001$) and FGCaMP ($p = 0.0045$), respectively. The $\Delta F/F_0$ response for FGCaMP6 was similar ($p = 0.9313$) to that of the original FGCaMP and 1.4-fold higher ($p = 0.0297$) than the response of the control GCaMP6s indicator. At 405 nm excitation, the $\Delta F/F_0$ values for all three indicators (FGCaMP5, FGCaMP6, and FGCaMP7) were similar and 1.4–1.6-fold less than that of FGCaMP ($p = 0.0243$, $p = 0.0230$, and $p = 0.0493$, respectively; Table 2). Hence, the FGCaMP7 indicator demonstrated the highest ionomycin-induced $\Delta F/F_0$ response in cultured mammalian cells among the three FGCaMP variants tested and GCaMP6s, while FGCaMP5 had the lowest $\Delta F/F_0$ response; this correlated with its lowest contrast and highest calcium affinity in vitro (Table 2).

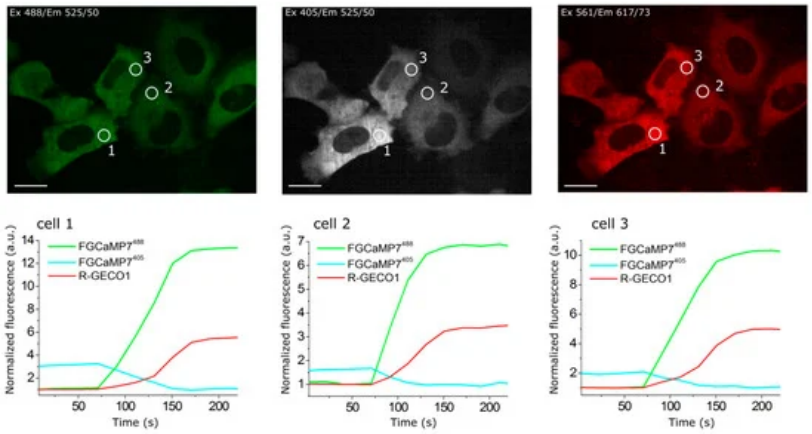

Figure 2. The response of the FGCaMP7 indicator to variations in cytoplasmic calcium concentration in HeLa Kyoto cells. (Upper panels) Confocal images of HeLa Kyoto cells co-expressing ratiometric indicator FGCaMP7 at 488 nm (left panel) and 405 nm (middle panel) excitations and red indicator R-GECO1 at 561 nm excitation (right panel). (Lower panels) The graphs illustrate changes in green fluorescence of FGCaMP7 at 488 nm (green lines) and 405 nm (cyan lines) excitations and red fluorescence of co-expressed R-GECO1 (red lines) GECI in response to 2.5 μM ionomycin. Changes in fluorescence are shown for three cells. The changes shown in graphs correspond to the areas indicated with white circles in the images in upper panels. Scale bar: 20 μm.

Figure S9. Response of FGCaMP **(a)**, FGCaMP5 **(b)**, and FGCaMP6 **(c)** GECIs to variations in the cytoplasmic calcium concentration in HeLa Kyoto cells. **(Upper panels)** Confocal images of HeLa Kyoto cells co-expressing respective indicator from FGCaMP series at 488 nm (left panels) and 405 nm (middle panels) excitations and red indicator R-GECO1 at 561 nm excitation (right panels). **(Lower panels)** The graphs illustrate changes in green fluorescence of the respective indicator from FGCaMP series at 488 nm (green lines) and 405 nm (cyan lines) excitations and red fluorescence of co-expressed R-GECO1 (red lines) GECI in response to 2.5 µM ionomycin. Changes in fluorescence of each FGCaMP indicator are shown for three cells. The changes shown in graphs correspond to the areas indicated with white circles in the images in upper panels. Scale bars: 20 µm.

Table 2. Characteristics of FGCaMP, FGCaMP5, FGCaMP6, FGCaMP7, and GCaMP6s GECIs responses to the addition of calcium ions to HeLa cells, to spontaneous activity in dissociated neuronal cultures, and electric stimulation of dissociated neuronal cultures.

		Protein				
		FGCaMP	**FGCaMP7**	**FGCaMP5**	**FGCaMP6**	**GCaMP6s**
$\Delta F/F_0$ in HeLa (% vs. R-GECO1)	**Ex405**	**62 ± 22 (*n* = 11)**	**42 ± 19 *p* = 0.0493 [a] (*n* = 10)**	**44 ± 16 *p* = 0.0243 [a] (*n* = 11)**	**40 ± 22 *p* = 0.0230 [a] (*n* = 10)**	**NA**
	Ex488	**162 ± 20 *p* = 0.0007 [b] (*n* = 11)**	**237 ± 81 *p* < 0.0001 [b] (*n* = 10)**	**87 ± 25 *p* = 0.0305 [b] (*n* = 11)**	**160 ± 55 *p* = 0.0297 [b] (*n* = 10)**	**113 ± 35 (*n* = 15)**

		Protein				
		FGCaMP	FGCaMP7	FGCaMP5	FGCaMP6	GCaMP6s
$\Delta F/F_0$ in neurons (% vs. R-GECO1)	Ex405	50 ± 20 (*n* = 12)	34 ± 13 *p* = 0.0267 [a] (*n* = 11)	19 ± 10 *p* = 0.0014 [a] (*n* = 11)	46 ± 37 *p* = 0.2412 [a] (*n* = 13)	NA
	Ex488	150 ± 53 *p* = 0.3299 [b] (*n* = 12)	142 ± 35 *p* = 0.4966 [b] (*n* = 10)	58 ± 25 *p* < 0.0001 [b] (*n* = 16)	143 ± 40 *p* = 0.3932 [b] (*n* = 14)	133 ± 58 (*n* = 17)
$\Delta R/R_0$ [c] in neurons (% vs. R-GECO1)		245 ± 110 *p* = 0.0030 [b] (*n* = 11)	219 ± 78 *p* = 0.0014 [b] (*n* = 10)	103 ± 42 *p* = 0.1436 [b] (*n* = 11)	231 ± 70 *p* = 0.0003 [b] (*n* = 13)	NA
rise half-time (s) [d]	Ex405	1.93 ± 0.62	1.36 ± 0.47	2.45 ± 1.09	2.01 ± 0.93	NA
	Ex488	2.08 ± 0.57	1.36 ± 0.47	2.01 ± 1.23	1.65 ± 0.71	1.14 ± 0.61
decay half-time (s) [e]	Ex405	3.56 ± 1.37	3.40 ± 0.72	5.78 ± 2.56	4.41 ± 2.18	NA
	Ex488	4.01 ± 1.65	3.84 ± 0.88	6.51 ± 2.50	4.89 ± 1.92	3.77 ± 1.27
$\Delta F/F_0$ per 1 AP in stimulated neurons (%)	Ex405	0.6 ± 0.4 [f] (*n* = 29)	2.1 ± 1.5 [g] *p* < 0.0001 [a] (*n* = 87)	1.1 ± 0.8 [f] (*p* = 0.0148) [a] (*n* = 17)	0.9 ± 0.9 [h] (*p* = 0.2678) [a] (*n* = 34)	NA
	Ex488	4.1 ± 1.7 [f] *p* < 0.0001 [b] (*n* = 29)	15.0 ± 7.5 [g] (*p* = 0.8805) [b] (*n* = 90)	3.5 ± 1.6 [f] *p* < 0.0001 [b] (*n* = 17)	7.3 ± 4.2 [h] *p* < 0.0001 [b] (*n* = 34)	15.0 ± 7.0 [g] (*n* = 50)
$\Delta R/R_0$ [c] per 1 AP in stimulated neurons (%)		5.4 ± 2.3 [f] *p* < 0.0001 [b] (*n* = 29)	20.3 ± 9.2 [g] (*p* = 0.0002) [b] (*n* = 86)	5.1 ± 2.4 [f] *p* < 0.0001 [b] (*n* = 17)	9.2 ± 4.7 [h] *p* < 0.0001 [b] (*n* = 34)	NA

5. Visualization of Spontaneous Activity in Neuronal Cultures Using Enhanced Versions of FGCaMP Indicator

We next compared the enhanced FGCaMP variants in their ability to monitor calcium dynamics during the spontaneous activity of live neurons. We co-transduced dissociated neuronal cultures isolated from mice pups with recombinant adeno-associated viral particles (rAAV) carrying FGCaMP5, FGCaMP6, FGCaMP7, FGCaMP, and GCaMP6s GECIs together with control red R-GECO1. We observed calcium oscillations in all cultures by day 11–17 in vitro (Figure 3 and Figure S10). In the case of the ratiometric FGCaMP series, calcium oscillations were detected with opposite fluorescence changes at 405 and 488 nm excitation, respectively (Figure 3 and Figure S10). The mean $\Delta F/F_0$ response (normalized to $\Delta F/F_0$ of R-GECO1) was similar for FGCaMP, FGCaMP6, and FGCaMP7 at 405 nm excitation. However, $\Delta F/F_0$ for FGCaMP5 was 2.6-fold lower ($p = 0.0014$) than that of FGCaMP, perhaps because the protein was partially bound to Ca^{2+} in resting neurons due to its lower K_d value of 98 nM, as compared to the K_d value of 460 nM for FGCaMP. At 488 nm excitation, the mean normalized $\Delta F/F_0$ responses for FGCaMP7 and FGCaMP6 were comparable to that of FGCaMP ($p = 0.8026$ and $p = 0.8895$, respectively) and GCaMP6s ($p = 0.4966$ and $p = 0.3932$, respectively; Table 2). The mean normalized $\Delta F/F_0$ for FGCaMP5 at 488 nm excitation was 2.3–2.6-fold lower ($p < 0.0001$) than $\Delta F/F_0$ for FGCaMP, FGCaMP6, FGCaMP7, and GCaMP6s. Finally, we estimated ratiometric $\Delta R/R_0$ responses for the FGCaMP5, FGCaMP6, and FGCaMP7 indicators normalized to $\Delta F/F_0$ of R-GECO1 and compared them to $\Delta R/R_0$ for the original FGCaMP and $\Delta F/F_0$ for GCaMP6s. The mean normalized $\Delta R/R_0$ for FGCaMP7 was 1.6-fold higher ($p = 0.0014$) than $\Delta F/F_0$ of GCaMP6s, comparable to $\Delta R/R_0$ of FGCaMP ($p = 0.3054$) and FGCaMP6 ($p = 0.6803$), and 2.1-fold higher ($p = 0.0002$) than $\Delta R/R_0$ of FGCaMP5 (Table 2). Hence, during the spontaneous activity of neuronal cultures, FGCaMP7 revealed $\Delta F/F_0$ or $\Delta R/R_0$ responses similar or superior to those for other FGCaMP variants, FGCaMP, and GCaMP6s.

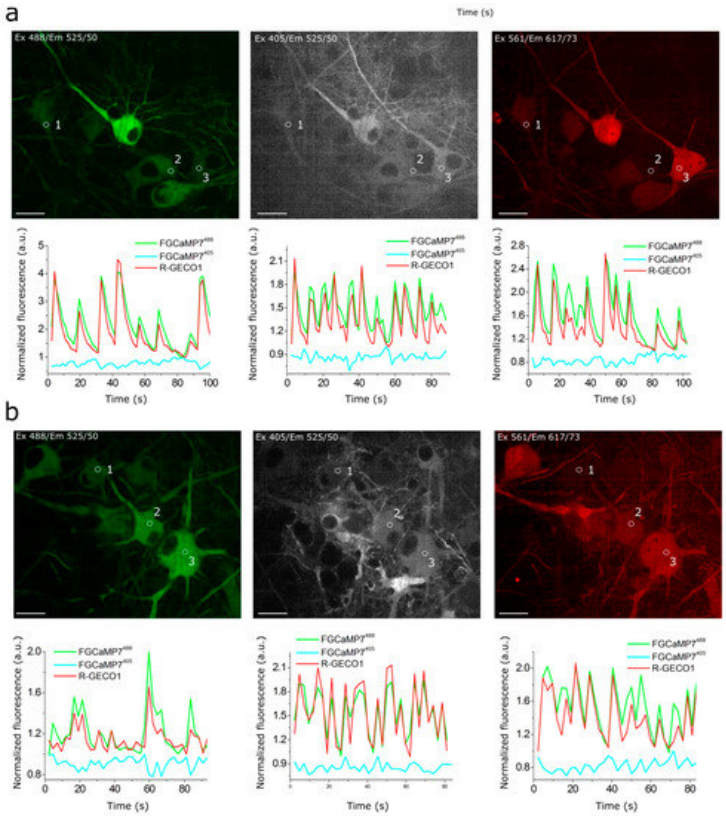

Figure 3. Responses of FGCaMP7 indicator to variations in cytoplasmic calcium concentration in cultured neurons. (**a**,**b**, upper panels) Confocal images of neurons co-expressing ratiometric indicator FGCaMP7 at 488 nm (left panel) and 405 nm (middle panel) excitations and red indicator R-GECO1 at 561 nm excitation (right panel). (**a**,**b**, lower panels) The graphs illustrate changes in green fluorescence of FGCaMP7 at 488 nm (green lines) and 405 nm (cyan lines) excitations and red fluorescence of co-expressed R-GECO1 (red lines) GECI as a result of spontaneous activity in neuronal cultures. Changes in fluorescence are shown for six neurons. The changes shown in graphs correspond to the areas indicated with white circles in the images in upper panels. Scale bar: 20 µm.

When comparing mean rise half-times at 488 nm excitation, the rise of FGCaMP7 fluorescence was slightly faster (1.36 ± 0.47 s) than the rise of the FGCaMP fluorescence (2.08 ± 0.57 s) and the other FGCaMP variants (FGCaMP5: 2.01 ± 1.23 s; FGCaMP6: 1.65 ± 0.71 s) and slightly slower than the rise of GCaMP6s fluorescence (1.14 ± 0.61 s). FGCaMP5 was the slowest indicator, with mean decay half-time values of 6.51 ± 2.50 and 5.78 ± 2.56 s at 488 and 405 nm excitation, respectively. Decay half-times for the FGCaMP7 (3.84 ± 0.88 and 3.40 ± 0.72 s at 488 and 405 nm excitation, respectively), FGCaMP (4.01 ± 1.65 and 3.56 ± 1.37 s at 488 and 405 nm excitation, respectively), and GCaMP6s (3.77 ± 1.27 s) GECIs were similar. Mean rise and decay half-times for the control co-expressed R-GECO1 indicator were similar to the respective half-times of FGCaMP7 ($t_{1/2}^{rise}$ R-GECO1 = 1.73 ± 0.63 s, $t_{1/2}^{decay}$ R-GECO1 = 4.17 ± 1.45 s).

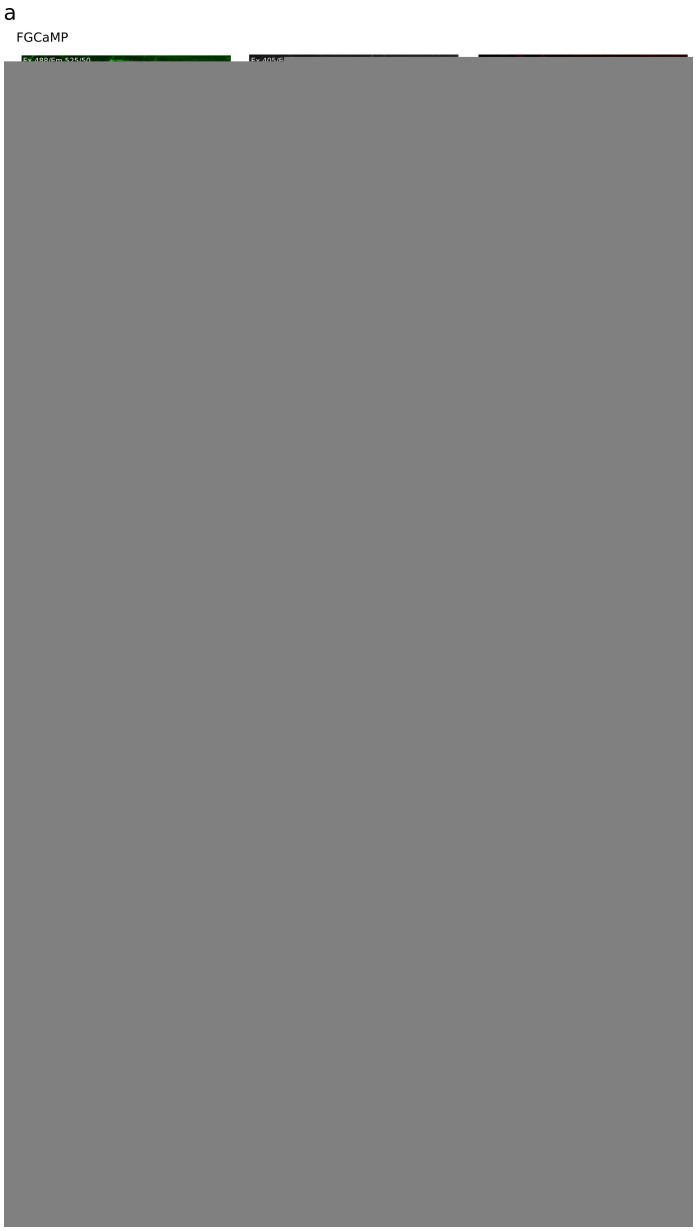

Figure S10. Response of FGCaMP **(a**), FGCaMP5 **(b)** and FGCaMP6 **(c)** GECIs to variations in the cytoplasmic calcium concentration in cultured neurons. **(Upper panels)** Confocal images of neurons co-expressing respective indicator from FGCaMP series at 488 nm (left panels) and 405 nm (middle panels) excitations and red indicator R-GECO1 at 561 nm excitation (right panels). **(Lower panels)** The graphs illustrate changes in green fluorescence of the respective indicator from FGCaMP series at 488 nm (green lines) and 405 nm (cyan lines) excitations and red fluorescence of co-expressed R-GECO1 (red lines) GECI as a result of spontaneous activity in neuronal cultures. Changes in fluorescence of each FGCaMP indicator are shown for three neurons. The changes shown in graphs correspond to the areas indicated with white circles in the images in upper panels. Scale bars: 20 µm.

Both FGCaMP7 and GCaMP6s indicators demonstrated even distribution in the cytosol of neurons, however R-GECO1 indicator revealed puncta-like aggregates during prolonged expression in neuronal cultures (Figure S11). This difference may be attributed to different fluorescent domains utilized in FGCaMP7 and GCaMP6s (EGFP fluorescent domain) as compared to R-GECO1 (mApple fluorescent domain). Puncta formation was attributed to lysosomes [25], therefore autophagy should adjust the number of these puncta [26].

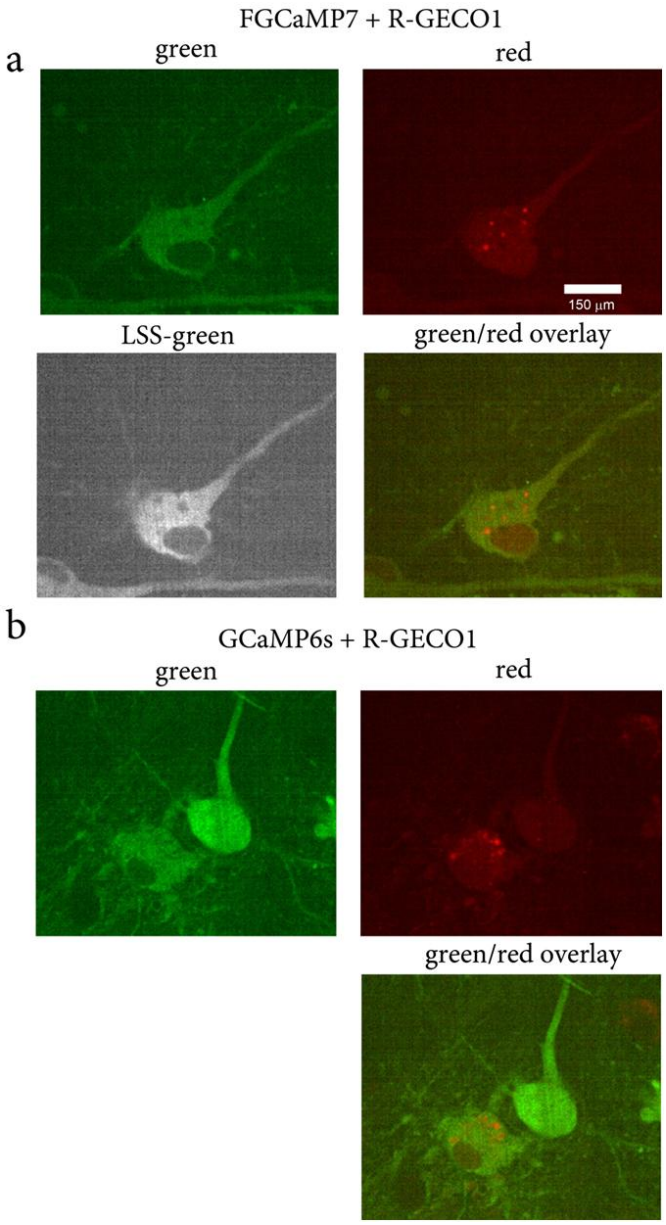

Figure S11. Localization of FGCaMP7 **(a)** and GCaMP6s **(b)** GECIs co-expressed with R-GECO1 in the cultured neurons. Confocal images of neurons co-expressing respective green indicator at 488 nm (green) and/or 405 nm (LSS-green) excitations with even distribution and red indicator R-GECO1 at 561 nm excitation (red) with uneven puncta-like distribution. Cultures were imaged on DIV 13 **(a)** and 16 **(b)**. Scale bar: 150 μm.

Hence, all three enhanced FGCaMP variants were able to visualize spontaneous calcium activity in neuronal culture. According to the rise and decay half-times values—as well as to the $\Delta F/F_0$ and $\Delta R/R_0$ response values—during spontaneous neuronal activity, FGCaMP7 was chosen as the best variant among them. Its normalized ratiometric $\Delta R/R_0$ response was 1.6-fold higher (p = 0.0014) than the normalized $\Delta F/F_0$ response for GCaMP6s.

6. Responses of Improved FGCaMP Indicators to External Electric Stimulation of Neuronal Cultures

We next compared the responses of the enhanced FGCaMP variants, control FGCaMP, GCaMP6s, and R-GECO1 GECIs during external electric field stimulation of neuronal cultures. FGCaMP variants were co-expressed in neuronal cultures together with reference red R-GECO1 [24]. FGCaMP and GCaMP6s GECIs were used as controls. The number of APs induced by 150–300 external electric field pulses were evaluated according to the $\Delta F/F_0$ changes of co-expressed R-GECO1, assuming linearity of its response and 4% $\Delta F/F_0$ value at 1 AP stimuli [27].

All indicators responded to trains of 1–40 APs; except for FGCaMP and FGCaMP5, which started to sense trains from 10 APs and up (Figure 4a,b) and FGCaMP6, which responded to trains starting from 4 APs and up (Figure 4c). The green fluorescence in GCaMP6s-expressing neurons increased in response to electric field stimulation, while green fluorescence in neurons expressing ratiometric indicators FGCaMP, FGCaMP5, FGCaMP6, and FGCaMP7 increased at 488 nm excitation and decreased at 405 nm excitation. To compare the responses of enhanced FGCaMP variants, we estimated $\Delta F/F_0$ or $\Delta R/R_0$ values per 1AP, calculated as a slope of linear dependence of $\Delta F/F_0$ or $\Delta R/R_0$ vs. trains of 1–

40 APs in the case of FGCaMP7 and GCaMP6s, 4–40 APs in the case of FGCaMP6, and 10–40 APs in the case of FGCaMP5 and FGCaMP (Figure 4). The $\Delta F/F_0$ response per 1 AP for FGCaMP7 at 405 nm excitation was 1.9–3.5-fold higher ($p < 0.0001$) than responses of FGCaMP5, FGCaMP6, and control FGCaMP (Table 2). At 488 nm excitation, $\Delta F/F_0$ response per 1AP for FGCaMP7 was 3.7- ($p < 0.0001$), 4.3- ($p < 0.0001$), and 2.1-fold ($p < 0.0001$) higher than the responses of FGCaMP, FGCaMP5, and FGCaMP6, respectively (Table 2). At 488 nm excitation, $\Delta F/F_0$ response per 1 AP for FGCaMP7 was similar ($p = 0.8805$) to that of GCaMP6s (Table 2). We also compared ratiometric $\Delta R/R_0$ responses per 1AP for enhanced FGCaMP variants with the respective $\Delta F/F_0$ value for GCaMP6s (Figure 4f and Table 2). The $\Delta R/R_0$ response per 1 AP for the FGCaMP7 variant with highest contrast in vitro was 3.8- ($p < 0.0001$), 4.0- ($p < 0.0001$), and 2.2-fold ($p < 0.0001$) higher than respective values for FGCaMP, FGCaMP5, and FGCaMP6, respectively. The $\Delta R/R_0$ response per 1 AP for FGCaMP7 was 1.4-fold higher ($p = 0.0002$) than the respective $\Delta F/F_0$ response per 1 AP for GCaMP6s (Table 2).

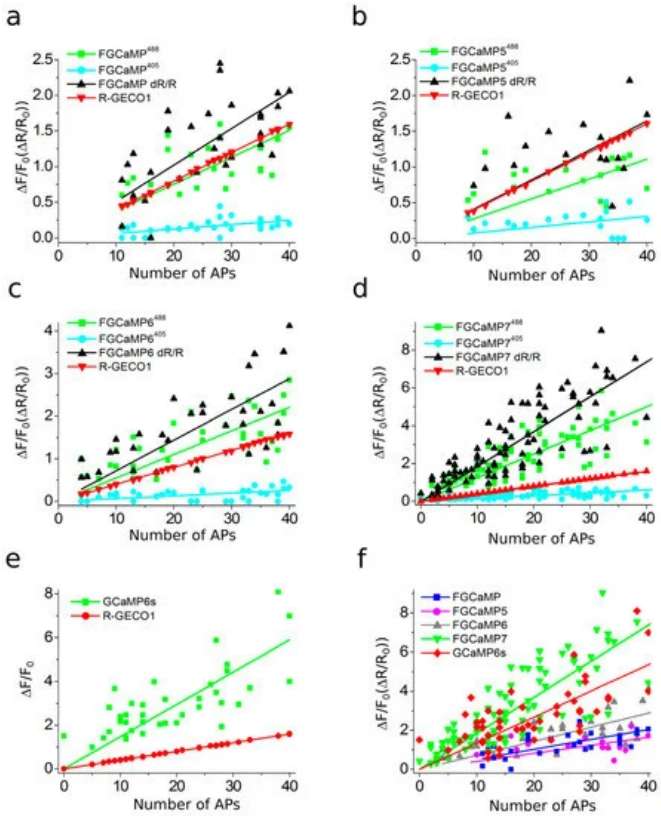

Figure 4. Fluorescence changes in cultured neurons co-expressing FGCaMP series and R-GECO1 in response to electric stimulation. (**a**–**e**) Fluorescence changes ($\Delta F/F_0$ and $\Delta R/R_0$) of FGCaMP, FGCaMP5, FGCaMP6, FGCaMP7, and GCaMP6s GECIs in response to external electric stimulation of neuronal cultures as a function of APs. APs were calculated by normalization of $\Delta F/F_0$ of co-expressed R-GECO1 to the 4% value, which is induced at 1 AP stimuli of R-GECO1, and assuming linear dependence of R-GECO1 response vs. APs [27]. (**f**) Ratiometric changes ($\Delta R/R_0$) for FGCaMP, FGCaMP5, FGCaMP6, FGCaMP7, and fluorescence change ($\Delta F/F_0$) for GCaMP6s GECIs.

Thus, according to the external electric field stimulation of neuronal cultures, the enhanced FGCaMP variants, similarly to control FGCaMP and GCaMP6s GECIs, demonstrated linear dependence of ΔF/F response in the range of 0–40 APs. The FGCaMP7 indicator outperformed the FGCaMP progenitor and FGCaMP5/FGCaMP6 indicators, in terms of larger $\Delta F/F_0$ and $\Delta R/R_0$ responses. The $\Delta F/F_0$ response per 1 AP for FGCaMP7 at 488 nm excitation was similar to that of the GCaMP6s control, while ratiometric $\Delta R/R_0$ response per 1 AP for FGCaMP7 was 1.4-fold higher ($p = 0.0002$) than $\Delta F/F_0$ per 1 AP for GCaMP6s. The FGCaMP7 variant was considered as best and chosen for further characterization in vitro, in mammalian cells, and in vivo.

7. Characterization of Truncated Versions (with Deleted M13-Like Peptide) of FGCaMP7 and GCaMP6s Indicators In Vitro and in HeLa Cells

To suggest the mechanism of fluorescence changes of the FGCaMP7 and GCaMP6s calcium indicators caused by calcium ion binding and to assess the possible interactions between these indicators and the intracellular environment, we constructed truncated versions of FGCaMP7 and GCaMP6s with deleted M13-like peptide (called FGCaM7 and GCaM6s, respectively) and studied their responses to calcium ions in vitro as purified proteins and in the cytosol of mammalian cells. These truncated versions, as purified proteins, practically did not respond to the addition of calcium ions in the range

of 39–2000 µM free-calcium ion concentrations (Table S5). Hence, the CaM domain binding to calcium ions does not evoke fluorescent changes in the FGCaMP7 and GCaMP6s indicators, per se. It is likely that only subsequent M13-like peptide binding with the calcium-saturated CaM domain is translated into the fluorescence response of these indicators.

Table S5. In vitro $\Delta F/F_0$ response of truncated versions (with deleted M13-like peptide) of the purified FGCaM7 and GCaM6s indicators to the saturating calcium ion concentrations.

Indicator	$\Delta F/F_0$, %		
	39 µM [a]	820 µM [a]	2000 µM [a]
FGCaM7	-4 ± 10	-13 ± 6	-16 ± 2
GCaM6s	5 ± 18	-9 ± 18	10 ± 12

[a] 39, 820, and 2000 µM free calcium concentration corresponds to the buffer supplemented with 10 mM CaEGTA, 10 mM NTA or 2 mM $CaCl_2$, respectively. Data were averaged across 3–6 repeats. SD is shown.

To assess the possible interactions of the FGCaMP7 and GCaMP6s proteins with the intracellular environment, we analyzed the responses of the FGCaM7 and GCaM6s truncated versions to ionomycin-induced calcium ion elevations in HeLa cells. The FGCaM7 and GCaM6s truncated versions transiently expressed in the HeLa cells had an even distribution in the cytosol of the cells (Figure 5a,b, respectively). FGCaM7 practically did not respond to the elevation of calcium ions induced by ionomycin addition, with $\Delta F/F_0$ values of 6.5 ± 2.4% (Figure 5a,c,d). However, GCaM6s sensed the ionomycin-induced elevation of calcium ions, with an $\Delta F/F_0$ response of 139 ± 62% (Figure 5b–d). Although this response was 4.3-fold lower ($p < 0.0001$), as compared to the $\Delta F/F_0$ response for the full-length GCaMP6s of 600 ± 333% under the same conditions, it was 21-fold larger ($p < 0.0001$) than that of FGCaM7. Taking into account that purified FGCaM7 and GCaM6s proteins practically did not respond to saturating calcium ion concentrations, we concluded that the CaM part of the GCaM6s protein interacted with intracellular proteins, as opposed to that in the FGCaM7 indicator. Earlier, the fluorescence recovery after photobleaching (FRAP) experiments demonstrated that the progenitor of the FGCaMP7 indicator, FGCaMP, was freely diffusible in the cytoplasm of HeLa cells at physiological Ca^{2+} concentrations, but that about 30% of GCaMP6s and G-GECO1.2 were not freely diffusible, suggesting that they may become bound to CaM or other cellular proteins [1]. Therefore, the GCaM6s protein is prone to interaction with intracellular proteins, in contrast to the FGCaM7 protein. We speculated that this difference may be attributed to the fungal origin of the CaM part in the FGCaM7 indicator, which has a different amino acid sequence than metazoan CaM. Overall, the M13-like peptide complex formation with calcium-bound CaM, rather than calcium ion binding by CaM domain, was translated into the fluorescence response of the GCaMP6s and FGCaMP7 indicators; in mammalian cells, the CaM domain of the FGCaMP7 indicator practically did not interact with intracellular proteins, in contrast to the CaM domain of the GCaMP6s indicator.

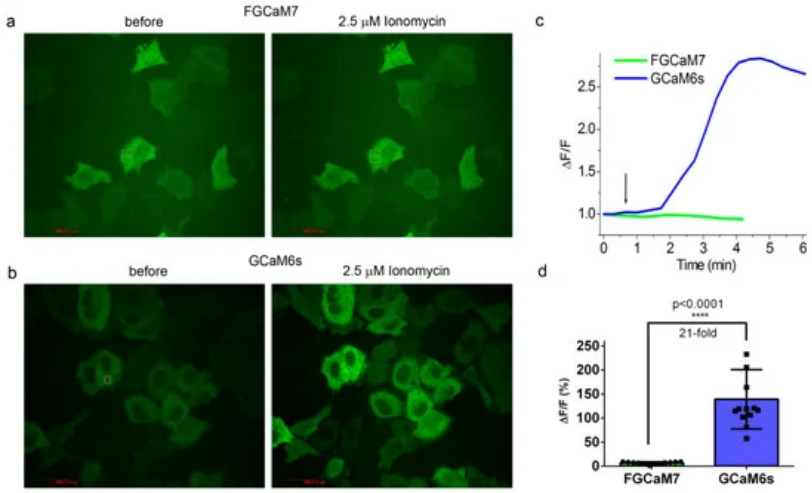

Figure 5. Calcium-dependent response of the truncated versions (with deleted M13-like peptide) of the FGCaMP7 and GCaMP6s indicators in HeLa cells. Confocal images of HeLa cells expressing FGCaM7 (**a**) and GCaM6s (**b**) before and after addition of 2.5 μm ionomycin. (**c**) Graph illustrating calcium-dependent change in $\Delta F/F_0$ for FGCaM7 (green) and GCaM6s (blue). Addition of 2.5 μm ionomycin is depicted by black arrow. (**d**) Averaged ionomycin-evoked $\Delta F/F_0$ responses for the FGCaM7 (n = 12) and GCaM6s (n = 13) trancated indicators.

8. In Vivo Imaging of Hippocampal Neuronal Activity in Freely Moving Mice Using NVista Miniscope and FGCaMP7 Calcium Indicator

To validate the in vivo application of the FGCaMP7 indicator using one-photon non-ratiometric imaging, we performed in vivo calcium imaging with an NVista head-mounted microscope (Figure 6a) and compared the amplitudes and kinetics of spikes detected during specific and non-specific activities of neurons in the CA1 field of the hippocampus while mice explored an O-shaped track with landmarks. The FGCaMP7 indicator was delivered into CA1 hippocampal neurons of 1–2 month-old mice using rAAVs carrying NES-FGCaMP under CAG promoter. Several weeks after lens probe implantation, we recorded neuronal activity in the hippocampus of the mice while they explored an O-shaped track with landmarks. Using the MIN1PIPE procedure pipeline [28] and manual inspection, we successfully identified active cells and extracted respective calcium activity $\Delta F/F_0$ traces. An example of typical neuronal activity for eight neurons is shown in Figure 6b. Averaged peak $\Delta F/F_0$ for FGCaMP7 was 1.0 ± 1.2, which was 2.1-fold lower (p < 0.0001) than averaged $\Delta F/F_0$ for GCaMP6s (Figure 6c and Table S6). Averaged rise and decay half-times for spikes detected for FGCaMP7 (0.97 ± 0.60 and 3.07 ± 0.80 s, respectively) were 1.3- (p = 0.0002) and 1.2-fold (p < 0.0001) longer than the respective times of the GCaMP6s indicator (0.76 ± 0.49 and 2.54 ± 0.94 s, respectively; Table S6). Therefore, the FGCaMP7 indicator detected hippocampal neuronal activity with slightly less sensitivity and resolution than the control GCaMP6s.

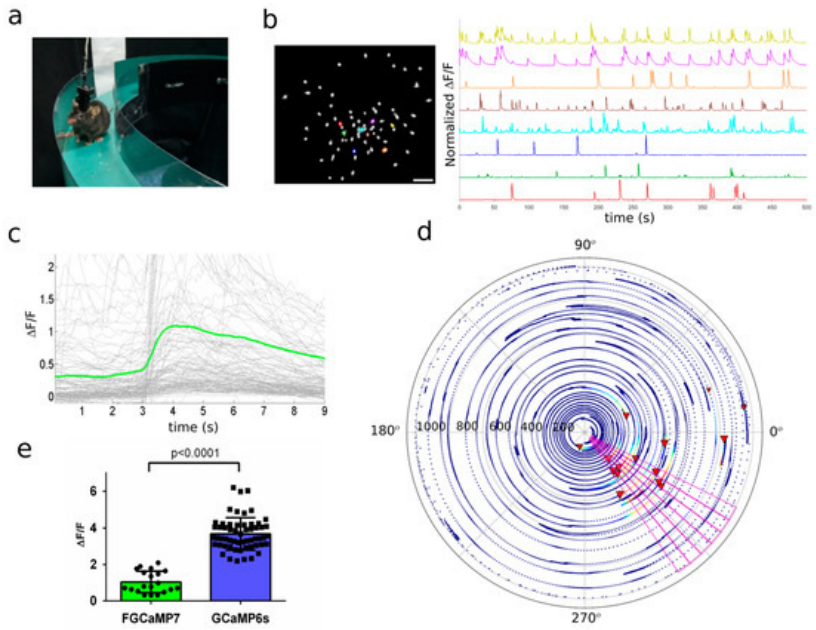

Figure 6. In vivo neuronal Ca^{2+} activity in the hippocampus of freely behaving mice visualized using FGCaMP7 and an nVista HD miniscope. (**a**) Photo of O-shaped track and mouse which explores it with an nVista HD miniscope mounted on its head. (**b**) Spatial filter and sample traces obtained from a 15-min imaging session of freely behaving mouse expressing FGCaMP7 GECI. $\Delta F/F_0$ values were normalized to the maximal $\Delta F/F_0$ for each trace. Scale bar: 100 μm. (**c**) Mean spike for FGCaMP7 calcium indicator; spikes above the 4 MAD threshold and not less than 50% of maximal trace value were aligned at the start of the peak (3 s). (**d**) Example of the circular plot for FGCaMP7 mouse trajectory during the exploration of circular track, synchronized with the spikes of a place cell (red triangles). Radial: time, s; angular: intrack position, degrees. (**e**) Averaged $\Delta F/F_0$ responses for space-evoked activity across place neuronal cells (n = 4, FGCaMP7; n = 5, GCaMP6s) in the CA1 area of the hippocampus for the FGCaMP7 and GCaMP6s indicators. The FGCaMP7 and GCaMP6s indicators were delivered to the hippocampus with rAAVs carrying AAV-CAG-NES-FGCaMP7/GCaMP6s.

Table S6. Comparison of calcium responses in neurons expressing FGCaMP7 and GCaMP6s indicators in hippocampus of freely moving mice registered with nVista HD miniscope in vivo.

Properties	Indicators	
	FGCaMP7	GCaMP6s
Number of mice	2	4
Number of active cells [a]	142	436
Number of spikes detected	135	316
Rise half-time, s [b]	0.97 ± 0.60 (p = 0.0002)	0.76 ± 0.49
Decay half-time, s [b]	3.07 ± 0.80 (p < 0.0001)	2.54 ± 0.94
Peak DF/F_0 [c]	1.0 ± 1.2 (p < 0.0001)	2.1 ± 1.8

[a] Only spikes exceeding 4MAD threshold and not less than 50% of maximum value of the trace were taken into account.

[b] Rise and decay half-times were calculated as time intervals between the peak of the mean spike and half-peak at front and back slopes of the spike.

[c] Peak DF/F_0 is given in MIN1PIPE units, which are DF/F_0 units after normalization and registration.

[b-c] Mean values ± standard error of mean are given. Analysis of calcium imaging data was performed as previously described [24].

p value shows statistical difference between the respective values for NCaMP7 and GCaMP6s control indicator.

We could not reveal a noticeable difference between the FGCaMP7 and GCaMP6s indicators according to the appearance of cells having an unusual shape and intracellular aggregates even upon prolonged in vivo expression of these indicators in hippocampus of mice (Figure S12). A separate study with better microscopic resolution and more statistics is needed to identify possible difference in cellular toxicity between FGCaMP7 and GCaMP6s.

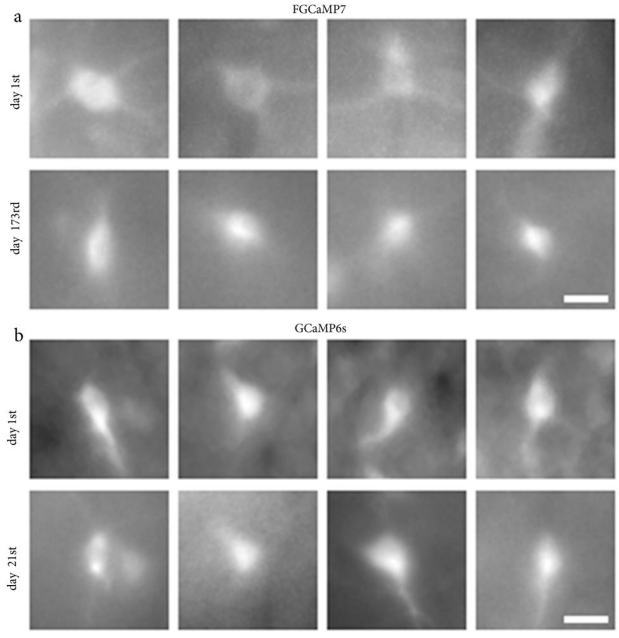

Figure S12. Examples of localization of FGCaMP7 **(a)** and GCaMP6s **(b)** GECIs expressed in the hippocampus of mice. Examples of individual cells expressing the FGCAMP7 (**a**) or GCaMP6s (**b**) indicators, which were imaged with the NVista HD miniscope at the start of the experiment (upper row) and 173 (a) or 21 (**b**) days later (bottom row, different cells within the same animal and field of view). Scale bar: 25 µm.

We next compared the ability of the FGCaMP7 and GCaMP6s indicators to visualize the location-specific activity of CA1 cells using an nVista miniscope [13]. We correlated the neuronal calcium activity in the CA1 area of the hippocampus while the mouse moved through an O-shaped track with landmarks (Figure 6a). As a result, using both indicators, we identified the neurons that were specifically activated in certain parts of the track (an example of an FGCaMP7-labeled place cell is shown in Figure 6d, as well as Videos S1 and S2). The ΔF/F responses of FGCaMP7 (1.0 ± 0.6) averaged across the space-specific activity of neuronal place cells were 3.7-fold lower ($p < 0.0001$) than the respective responses of the GCaMP6s indicator (3.7 ± 0.9) (Figure 6e). Thus, FGCaMP7 detected both non-specific and specific neuronal activity with an ΔF/F response 2.1–3.7-fold lower than GCaMP6s.

9. In Vivo Imaging of Hippocampal Neuronal Ensembles in Mice during Food Intake Using NVista Miniscope and FGCaMP7 Calcium Indicator

To demonstrate the capability of the FGCaMP7 indicator to reveal neuronal ensembles, we performed in vivo calcium imaging of the mouse hippocampus using an NVista head-mounted microscope during food intake sessions. The FGCaMP7 indicator was delivered into CA1 hippocampal neurons using rAAVs carrying NES-FGCaMP under CAG promoter. Ca^{2+} imaging was performed for 1 h in the home cage with two weighed cups of familiar powdered food after food deprivation for 24 h (Figure 7a). Based on a calcium activity $\Delta F/F_0$ trace extraction routine described earlier [29], we correlated neuronal activity of the CA1 hippocampus with the trajectory of the mouse (Figure 7b) and detected moments of transitions to the food cup area (Figure 7c). To analyze neuronal response dynamics during the transition to the food cup area, we averaged z-scored neuronal Ca^{2+} responses for each neuron in a time window from 2 s before the transition to 5 s after [30]. The mean responses of all neurons from two mice were clustered into three groups using k-means (Figure 7d), which revealed a generally activated ensemble (40% of neurons), a generally inhibited ensemble (19% of neurons), and an ensemble with neutral responses (Figure 7e). The mean z-scored $\Delta F/F_0$ response to cup area-entry transitions showed an increase by 0.9 ($p < 0.0001$) for the activated ensemble and a decrease by 0.3 ($p < 0.0001$) for the inhibited ensemble (Figure 7f). Similarly, three types of ensembles in the amygdala of mice were observed in other types of behavioral tasks [30][31]. The mean z-scored $\Delta F/F_0$ responses for these ensembles were the same, as compared to our data. Overall, using the FGCaMP7 indicator and population analysis of neuronal activity, we identified three types of neuronal ensembles in the hippocampus of mice during food intake.

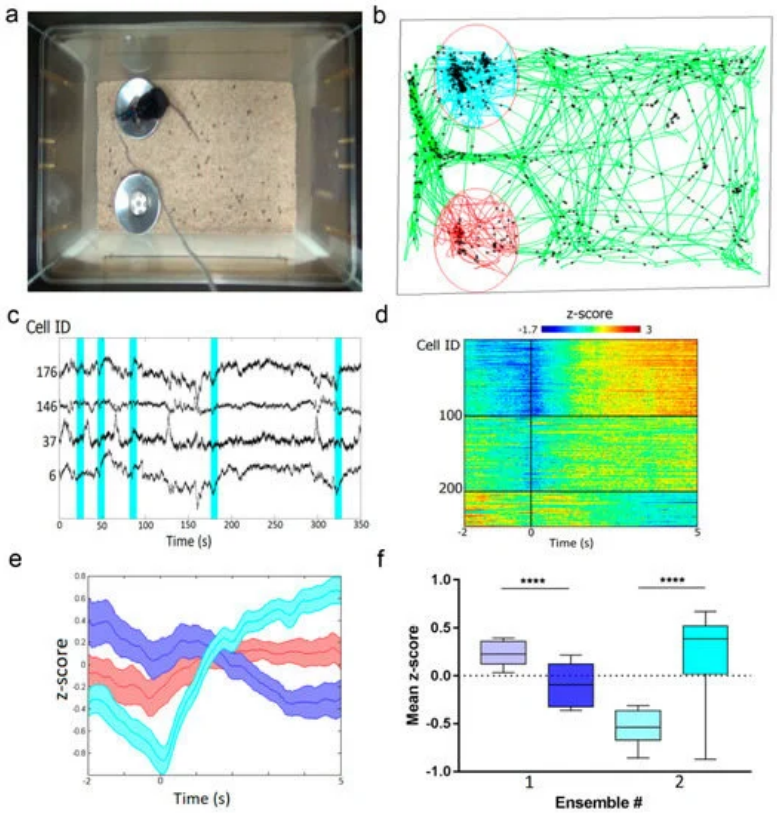

Figure 7. In vivo neuronal Ca2+ activity in mouse hippocampus during food intake visualized using FGCaMP7 and an nVista HD miniscope. (**a**) Photo of the mouse with an nVista HD miniscope mounted on its head during food intake. (**b**) Mouse trajectory for 1-h imaging session (green) with spikes from all detected neurons (black stars), red and cyan curves —trajectory in the area of cups. Context size: 40 cm by 30 cm. (**c**) Example normalized ΔF/F0 Ca2+ signals for four individual neurons recorded during the session. Cyan areas show time windows 2 s before entering the cup area and 5 s after. (**d**) Mean responses of clustered groups of neurons upon cup area-entry transitions (*n* = 253 neurons from two mice; number of entries, 17 and 24). Zero marks cup area-entry time points. Cells were ordered according to k-means clustering. (**e**) Average cup area-entry responses of activated (cyan), inhibited (blue) and indifferent (red) ensembles. Lines indicate the average across neurons ± SEM. (**f**) Average z-score at 2 s time window before entering the cup area and 5 s after for activated (#1) and inhibited (#2) ensembles. *p* values less than 0.0001 are given four asterisks.

10. Two-Photon In Vivo Imaging of Visual Cortex in Awake Mice Expressing FGCaMP7 Calcium Indicator

To estimate the two-photon performance of the novel FGCaMP7 indicator in vivo, we assessed its response to spontaneous neuronal activity in awake mice under a two-photon microscope. rAAV particles of the FGCaMP7 indicator with NES signal were injected into the brain of mice pups at the age of P0–P1 using a Hamilton syringe. A month after viral infection, a cranial window was implanted and, one month later, two-photon imaging of spontaneous neuronal activity was performed in the L2/3 layer of the visual cortex in awake mice. FGCaMP7-expressing neurons were identified using both 800 and 960 nm excitation light, which excited protonated and anionic forms of the indicator, respectively. Both forms of FGCaMP7 demonstrated cytosolic nuclei-excluded expression (Figure 8a,b; left).

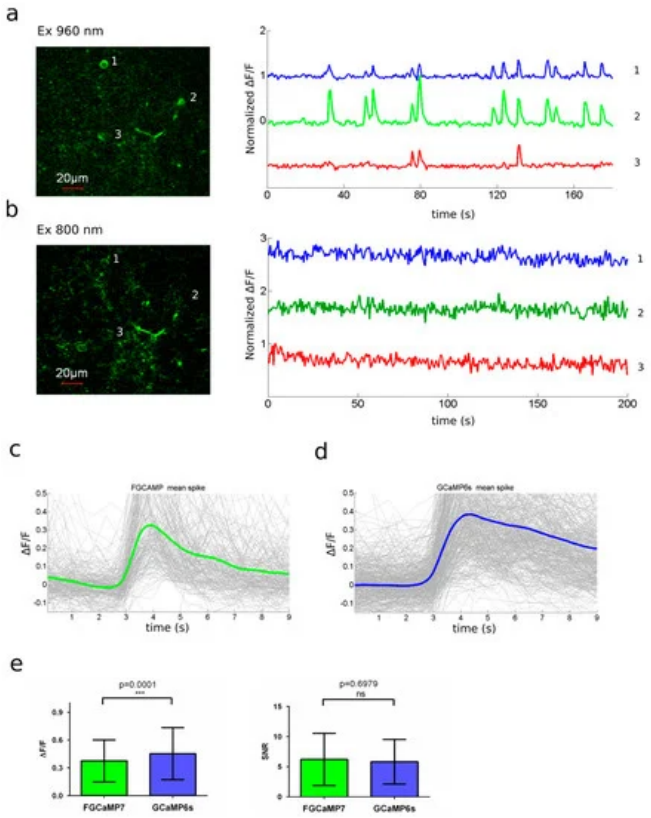

Figure 8. In vivo neuronal Ca^{2+} activity in the visual cortex of awake mice visualized using two-photon microscopy. (**a**,**b**) Two-photon images of V1 layer 2/3 neurons (left) and sample traces for marked neurons (right) acquired during their spontaneous activity at 960 nm (**a**) and 800 nm excitations (**b**) in the mice expressing FGCaMP7 calcium indicator. $\Delta F/F_0$ value was normalized to maximal $\Delta F/F_0$ for each trace. (**c**,**d**) Mean spike for the FGCaMP7 and GCaMP6s indicators; spikes with an amplitude above the 3 MAD threshold and not less than 50% of maximal trace value were aligned at the start of the peak (3 s). (**e**) Averaged peak $\Delta F/F_0$ responses and SNRs for spontaneous neuronal activity (*n* = 20, FGCaMP7; *n* = 14, GCaMP6s) 2/3-layer neurons of visual cortex for the FGCaMP7 and GCaMP6s indicators. *p* value equal to 0.0001 is given three asterisks.

Spontaneous neuronal activity was observed at a depth of 40–250 μm. An example of neuronal activity traces at 960 nm excitation is demonstrated in Figure 8a (right). Though we observed green fluorescence in FGCaMP7-expressing neurons at 800 nm excitation, we could not detect any fluorescence changes associated with Ca^{2+} dynamics in neurons using this

excitation light; perhaps due to the 3.5-fold lower $\Delta F/F_0$ response for the 400 nm absorbing form, as compared to the response for the 498 nm absorbing form in vitro (Figure 8b, right; Figure S13; and Table 1).

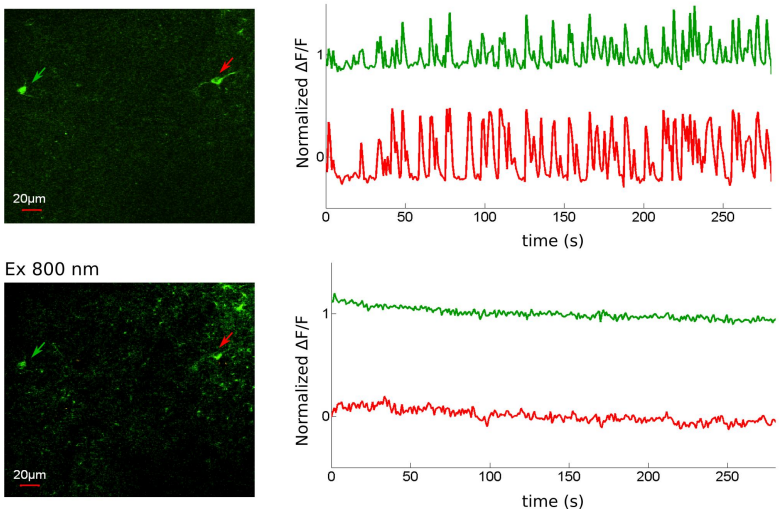

Figure S13. In vivo neuronal Ca^{2+} activity in visual cortex of awake mice vizualized using two-photon microscopy. **(left)** Two-photon images of V1 layer 2/3 neurons acquired during spontaneous activity at 960 nm and 800 nm excitation, respectively, in the mice expressing FGCaMP7 calcium indicator. **(right)** Sample traces obtained for neurons marked at images at 960 nm and 800 nm excitations. $\Delta F/F_0$ value normalized to maximal $\Delta F/F_0$ for each trace.

Two-photon excitation of the blue-shifted absorption peak of the NIR-GECO1 indicator also did not result in the observation of fluorescence changes associated with neuronal calcium dynamics in cultured neurons and in vivo [32]. At 960 nm excitation, we observed neuronal activity-dependent changes in fluorescence of the FGCaMP7 anionic form, with a peak $\Delta F/F_0$ of 0.37 ± 0.23 (Figure 8c). In the case of GCaMP6s, peak $\Delta F/F_0$ was 0.45 ± 0.28 (Figure 8d), which was 1.2-fold higher (p = 0.0001) than that of FGCaMP7 (Figure 8e). Signal-to-noise ratios (SNR) were the same (p = 0.6979) for FGCaMP7 (6.22 ± 4.32) and GCaMP6s (5.82 ± 3.70) (Figure 8e). FGCaMP7 was 1.4–1.5-fold (p < 0.0001) faster, in terms of rise (1.06 ± 0.79 s) and decay (2.07 ± 1.09 s) half-times, when compared with the rise (1.58 ± 0.88 s) and decay (2.88 ± 1.16 s) half-times of GCaMP6s. Hence, the FGCaMP7 indicator could visualize spontaneous neuronal activity in the visual cortex of mouse brain in vivo using two-photon excitation of its anionic form with 960 nm light; in contrast to its second protonated form (excited with 800 nm two-photon light), which was fluorescent but did not respond to neuronal activity.

11. In Vivo Ratiometric Two-Color Imaging of Neuronal Activity in Zebrafish Using FGCaMP7

To test whether FGCaMP7 can report neuronal activity in vivo under one-photon ratiometric imaging, we transiently expressed NES-FGCaMP7 under the pan-neuronal promoter *elavl3* in zebrafish larvae and imaged spontaneous activity (see Methods). Both 400- and 498-forms of the FGCaMP7 indicator were observed using 405 and 488 nm excitation light, respectively (Figure 9a). The FGCaMP7 indicator was excluded from nuclei and observed in the soma and processes of neurons. We performed live-imaging to record spontaneous activity in nine neurons from six larvae. Fluorescence transients were observed for both forms (Figure 9b), except for the 400-form in one cell. We calculated the average peak $\Delta F/F_0$ value and rise/decay half-times for both forms across all imaged cells using the averaged calcium transient for each cell (Figure 9c,d). The average peak $\Delta F/F_0$ value at 488 nm excitation was 1.64 ± 0.87 (mean ± SEM), which was about 9.6-fold higher than the $\Delta F/F_0$ value of −0.17 ± 0.05 at 405 nm excitation. The average $\Delta R/R_0$ value for the ratio of the observed signals (488 nm signal over 405 nm signal) was 3.13 ± 1.98 (Figure 9d). The average rise and decay half-times were similar for both forms: $t_{1/2}^{on}$ 1.47 ± 0.31 s for 488 nm and 1.45 ± 0.29 s for 405 nm; while $t_{1/2}^{off}$ 6.25 ± 1.37 s for 488 nm and 7.19 ± 2.30 for 405 nm (Figure 9d). These results demonstrate that the FGCaMP7 indicator can be used to ratiometrically monitor calcium transients in vivo in larval zebrafish with a high signal-to-noise ratio.

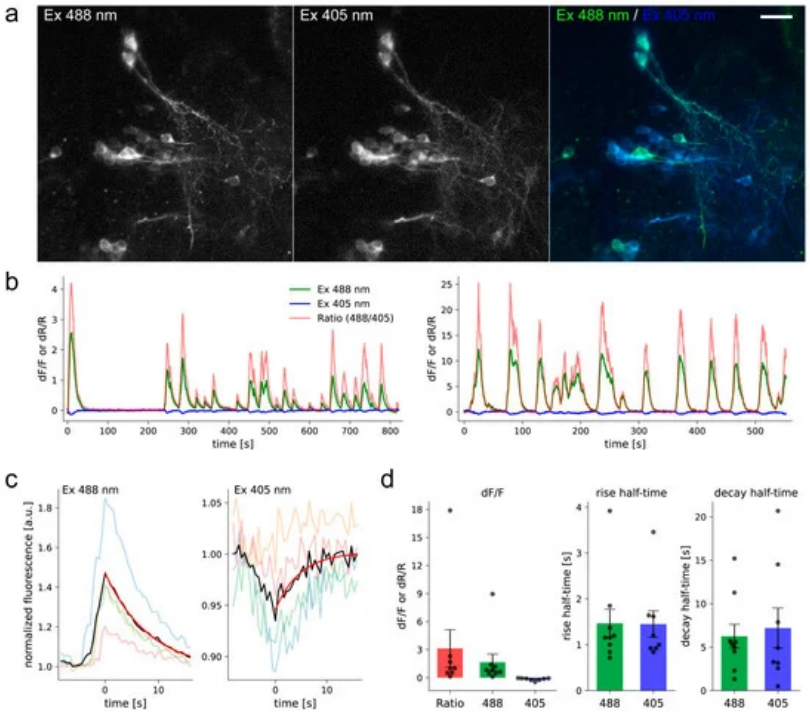

Figure 9. In vivo neuronal Ca^{2+} activity in larval zebrafish brain visualized using laser-scanning confocal microscopy. (**a**) NES-FGCaMP7 transiently expressed in the larval zebrafish brain. Maximum intensity projection image at 488 (left) or 405 (middle) nm excitation, and the merged image (right; 488 in green, 405 in blue). Scale bar: 20 µm. (**b**) Sample of $\Delta F/F_0$ and $\Delta R/R_0$ traces of spontaneous activity in 2 cells from 2 zebrafish larvae. Signal obtained at 488 and 405 nm excitation and their ratio (488/405) are shown in green, blue, and red lines, respectively. (**c**) Sample traces of spikes from 1 cell (pale color) and the averaged spike (black). Exponential (red) was fit to the decay of the averaged trace. (**d**) Mean of peak $\Delta F/F_0$ or $\Delta R/R_0$ (left), rise half-time (middle), and decay half-time (right) measured on averaged traces for 488 and 405 nm excitation and the ratio (488/405). Each dot represents a value measured in 1 cell. *n* = 9 for 488 nm excitation, 8 for 405 nm excitation and the ratio. Error bars indicate SEM.

References

1. Natalia V. Barykina; Oksana M. Subach; Kiryl D. Piatkevich; Erica E. Jung; Alexey Malyshev; Ivan Smirnov; Andrey O. Bogorodskiy; Valentin Borshchevskiy; Anna M. Varizhuk; Galina E. Pozmogova; et al. Green fluorescent genetically enc oded calcium indicator based on calmodulin/M13-peptide from fungi. *PLOS ONE* **2017**, *12*, e0183757, 10.1371/journal. pone.0183757.
2. Jessica L. Gifford; Michael P. Walsh; Hans J. Vogel; Structures and metal-ion-binding properties of the Ca2+-binding he lix–loop–helix EF-hand motifs. *Biochemical Journal* **2007**, *405*, 199-221, 10.1042/bj20070255.
3. Tsien, R.Y; The green fluorescent protein. *Annu. Rev. Biochem.* **1998**, *67*, 509–544, .
4. Haruki Niwa; Satoshi Inouye; Takashi Hirano; Tatsuki Matsuno; Satoshi Kojima; Masayuki Kubota; Mamoru Ohashi; Fre derick I. Tsuji; Chemical nature of the light emitter of the Aequorea green fluorescent protein. *Proceedings of the Nation al Academy of Sciences* **1996**, *93*, 13617-13622, 10.1073/pnas.93.24.13617.
5. Katjuša Brejc; Titia K Sixma; P. A. Kitts; S. R. Kain; R. Y. Tsien; M. Ormö; S. J. Remington; Structural basis for dual exci tation and photoisomerization of the Aequorea victoria green fluorescent protein. *Proceedings of the National Academy of Sciences* **1997**, *94*, 2306-2311, 10.1073/pnas.94.6.2306.
6. Needham, A.E. The Uniqueness of Biological Materials: International Series of Monographs in Pure and Applied Biolog y: Zoology; Elsevier Science: Amsterdam, The Netherlands, 2013.
7. Timothy I. Wood; David P. Barondeau; Chiharu Hitomi; Carey J. Kassmann; John Tainer; Elizabeth D. Getzoff; Defining the Role of Arginine 96 in Green Fluorescent Protein Fluorophore Biosynthesis†,‡. *Biochemistry* **2005**, *44*, 16211-1622 0, 10.1021/bi051388j.
8. David P. Barondeau; Christopher Putnam; Carey J. Kassmann; John Tainer; Elizabeth D. Getzoff; Mechanism and ener getics of green fluorescent protein chromophore synthesis revealed by trapped intermediate structures. *Proceedings of the National Academy of Sciences* **2003**, *100*, 12111-12116, 10.1073/pnas.2133463100.
9. Shounak Banerjee; Christian D. Schenkelberg; Thomas B. Jordan; Julia M. Reimertz; Emily E. Crone; Donna E. Crone; Christopher Bystroff; Mispacking and the Fitness Landscape of the Green Fluorescent Protein Chromophore Milieu. *Bio*

chemistry **2017**, *56*, 736-747, 10.1021/acs.biochem.6b00800.

10. M Ormö; A B Cubitt; K Kallio; L A Gross; R Y Tsien; § S. James Remington; Crystal structure of the Aequorea victoria gr een fluorescent protein. *Science* **1996**, *273*, 1392–1395, .
11. Gregor Jung; Jens Wiehler; Andreas Zumbusch; The Photophysics of Green Fluorescent Protein: Influence of the Key Amino Acids at Positions 65, 203, and 222. *Biophysical Journal* **2005**, *88*, 1932-1947, 10.1529/biophysj.104.044412.
12. D. A. Doronin; N. V. Barykina; Fedor V. Subach; Vladimir P. Sotskov; Viktor V. Plusnin; O. A. Ivleva; E. A. Isaakova; Ann a M. Varizhuk; Galina E. Pozmogova; Alexey Malyshev; et al. Genetically encoded calcium indicator with NTnC-like des ign and enhanced fluorescence contrast and kinetics.. *BMC Biotechnology* **2018**, *18*, 10, 10.1186/s12896-018-0417-2.
13. Natalia V. Barykina; Danila A. Doronin; Oksana M. Subach; Vladimir P. Sotskov; Viktor V. Plusnin; Olga A. Ivleva; Anna M. Gruzdeva; Tatiana A. Kunitsyna; Olga I. Ivashkina; Alexander Lazutkin; et al. NTnC-like genetically encoded calcium indicator with a positive and enhanced response and fast kinetics. *Scientific Reports* **2018**, *8*, 15233, 10.1038/s41598-0 18-33613-6.
14. Jacques Brocard; Sunita Rajdev; Ian J. Reynolds; Glutamate-induced increases in intracellular free Mg2+ in cultured c ortical neurons. *Neuron* **1993**, *11*, 751-757, 10.1016/0896-6273(93)90084-5.
15. Vadim Pérez Koldenkova; Takeharu Nagai; Genetically encoded Ca2+ indicators: Properties and evaluation. *Biochimic a et Biophysica Acta (BBA) - Molecular Cell Research* **2013**, *1833*, 1787-1797, 10.1016/j.bbamcr.2013.01.011.
16. Yufeng Zhao; Daniel Bushey; Yongxin Zhao; Eric R. Schreiter; D. Jed Harrison; Allan M. Wong; Robert E. Campbell; In verse-response Ca2+ indicators for optogenetic visualization of neuronal inhibition. *Scientific Reports* **2018**, *8*, 11758, 1 0.1038/s41598-018-30080-x.
17. Michael J Berridge; Peter Lipp; Martin Bootman; The versatility and universality of calcium signalling. *Nature Reviews Molecular Cell Biology* **2000**, *1*, 11-21, 10.1038/35036035.
18. Miguel Maravall; Zachary F. Mainen; B.L. Sabatini; K. Svoboda; Estimating intracellular calcium concentrations and buff ering without wavelength ratioing.. *Biophysical Journal* **2000**, *78*, 2655-2667, 10.1016/s0006-3495(00)76809-3.
19. Tsai-Wen Chen; Trevor J Wardill; Yi Sun; Stefan R. Pulver; Sabine Renninger; Amy Baohan; Eric R. Schreiter; Rex A. K err; Michael B. Orger; Vivek Jayaraman; et al. Ultrasensitive fluorescent proteins for imaging neuronal activity. *Nature* **2 013**, *499*, 295-300, 10.1038/nature12354.
20. Tobias Rose; Pieter M. Goltstein; Ruben Portugues; Oliver Griesbeck; Putting a finishing touch on GECIs. *Frontiers in Neuroscience* **2014**, *7*, 88, 10.3389/fnmol.2014.00088.
21. G Grynkiewicz; M Poenie; R Y Tsien; A new generation of Ca2+ indicators with greatly improved fluorescence propertie s. *Journal of Biological Chemistry* **1985**, *260*, 3440–3450, .
22. Hang Yao; Enbo Ma; Xiang-Qun Gu; G G Haddad; Intracellular pH regulation of CA1 neurons in Na+/H+ isoform 1 mut ant mice. *Journal of Clinical Investigation* **1999**, *104*, 637-645, 10.1172/jci6785.
23. Nathan C Shaner; Paul A Steinbach; Roger Y Tsien; A guide to choosing fluorescent proteins. *Nature Methods* **2005**, *2*, 905-909, 10.1038/nmeth819.
24. Yongxin Zhao; Satoko Araki; Jiahui Wu; Takayuki Teramoto; Yu-Fen Chang; Masahiro Nakano; Ahmed S. Abdelfattah; Manabi Fujiwara; Takeshi Ishihara; Takeharu Nagai; et al. An Expanded Palette of Genetically Encoded Ca2+ Indicator s. *Science* **2011**, *333*, 1888-1891, 10.1126/science.1208592.
25. Shen, Y.; Dana, H.; Abdelfattah, A.S.; Patel, R.; Shea, J.; Molina, R.S.; Rawal, B.; Rancic, V.; Chang, Y.F.; Wu, L.; et al. A genetically encoded Ca2+ indicator based on circularly permutated sea anemone red fluorescent protein eqFP578. *B MC Biology* **2018**, *16*, 9, .
26. Susmita Kaushik; Ana Maria Cuervo; The coming of age of chaperone-mediated autophagy. *Nature Reviews Molecular Cell Biology* **2018**, *19*, 365-381, 10.1038/s41580-018-0001-6.
27. Dana, H.; Mohar, B.; Sun, Y.; Narayan, S.; Gordus, A.; Hasseman, J.P.; Tsegaye, G.; Holt, G.T.; Hu, A.; Walpita, D.; et a l. Sensitive red protein calcium indicators for imaging neural activity. *Elife* **2017**, *5*, e12727, .
28. Jinghao Lu; Chunyuan Li; Jonnathan Singh-Alvarado; Zhe Charles Zhou; Flavio Fröhlich; Richard Mooney; Fan Wang; MIN1PIPE: A Miniscope 1-Photon-Based Calcium Imaging Signal Extraction Pipeline. *Cell Reports* **2018**, *23*, 3673-368 4, 10.1016/j.celrep.2018.05.062.
29. Natalia V. Barykina; Oksana M. Subach; Danila A. Doronin; Vladimir P. Sotskov; Marina A. Roshchina; Tatiana A. Kunits yna; Alexey Malyshev; Ivan Smirnov; Asya Azieva; Ilya S. Sokolov; et al. A new design for a green calcium indicator wit h a smaller size and a reduced number of calcium-binding sites. *Scientific Reports* **2016**, *6*, 34447, 10.1038/srep34447.
30. Grundemann, J.; Bitterman, Y.; Lu, T.; Krabbe, S.; Grewe, B.F.; Schnitzer, M.J.; Luthi, A; Amygdala ensembles encode behavioral states. *Science* **2019**, *364*, eaav8736, .

31. Xian Zhang; Bo Li; Population coding of valence in the basolateral amygdala. *Nature Communications* **2018**, *9*, 5195, 10.1038/s41467-018-07679-9.
32. Yong Qian; Kiryl D. Piatkevich; Benedict Mc Larney; Ahmed S. Abdelfattah; Sohum Mehta; Mitchell Murdock; Sven Gottschalk; Rosana S. Molina; Wei Zhang; Yingche Chen; et al. A genetically encoded near-infrared fluorescent calcium ion indicator. *Nature Methods* **2019**, *16*, 171-174, 10.1038/s41592-018-0294-6.